HHS Public Access

Author manuscript

Prog Neurobiol. Author manuscript; available in PMC 2023 September 01.

Published in final edited form as:

Prog Neurobiol. 2022 September ; 216: 102307. doi:10.1016/j.pneurobio.2022.102307.

α-Synucleinopathy Exerts Sex-Dimorphic Effects on the Multipurpose DNA Repair/Redox Protein APE1 in Mice and Humans

Kristin M. Miner[a], **Anuj S. Jamenis**[a], **Tarun N. Bhatia**[a], **Rachel N. Clark**[a], **Dhivyaa Rajasundaram**[b], **Sylvie Sauvaigo**[c], **Daniel M. Mason**[a], **Jessica M. Posimo**[a], **Nevil Abraham**[a], **Brett A. DeMarco**[a], **Xiaoming Hu**[d], **R. Anne Stetler**[d], **Jun Chen**[d], **Laurie H. Sanders**[e], **Kelvin C. Luk**[f], **Rehana K. Leak**[*,a]

[a]Graduate School of Pharmaceutical Sciences, Duquesne University, Pittsburgh, PA 15282, USA

[b]Department of Pediatrics, Rangos Research Center, UPMC Children's Hospital of Pittsburgh, PA 15224, USA

[c]LXRepair, Grenoble, France

[d]Department of Neurology, University of Pittsburgh, PA 15213, USA

[e]Department of Neurology, Duke University School of Medicine, Durham, NC 27710, USA

[f]Department of Pathology and Laboratory Medicine, University of Pennsylvania, Philadelphia, PA 19147, USA

Abstract

Lewy body disorders are characterized by oxidative damage to DNA and inclusions rich in aggregated forms of α-synuclein. Among other roles, apurinic/apyrimidinic endonuclease 1 (APE1) repairs oxidative DNA damage, and APE1 polymorphisms have been linked to cases of Lewy body disorders. However, the link between APE1 and α-synuclein is unexplored. We report that knockdown or inhibition of APE1 amplified inclusion formation in primary hippocampal cultures challenged with preformed α-synuclein fibrils. Fibril infusions into the mouse olfactory bulb/anterior olfactory nucleus (OB/AON) elicited a modest decrease in APE1 expression in the brains of male mice but an increase in females. Similarly, men with Lewy body disorders displayed lower APE1 expression in the OB and amygdala compared to women. Preformed fibril infusions of the mouse OB/AON induced more robust base excision repair of DNA lesions in females than males. No fibril-mediated loss of APE1 expression was observed in male mice when the antioxidant N-acetylcysteine was added to their diet. These findings reveal a potential sex-biased link between α-synucleinopathy and APE1 in mice and humans. Further studies are

[*]*Correspondence*: Rehana K. Leak, Ph.D., 407 Mellon Hall, Graduate School of Pharmaceutical Sciences, Duquesne University, 600 Forbes Ave, Pittsburgh, PA 15282, (412) 396-4734, leakr@duq.edu.

Authors' Contributions: Investigation, methodology, and biostatistical analyses: KMM, ASJ, TNB, RNC, DR, NA, SS, DM, JMP, BD, & RKL. Writing: KMM & RKL. Scientific feedback and revisions: TNB, ASJ, RNC, DR, SS, RAS, XH, JC, LHS, & KCL. Project administration, design, supervision, and funding acquisition: RKL.

Declaration of Competing Interest: The authors report no competing interests.

The authors have no conflicts to declare.

warranted to determine how this multifunctional protein modifies α-synuclein inclusions and, conversely, how α-synucleinopathy and biological sex interact to modify APE1.

Keywords

Dementia with Lewy bodies; Parkinson's disease; Synuclein; REF-1; Fibrils

1. Introduction

A majority of oxidative damage to DNA is sublethal and elicits a robust repair response, but when repair systems fail repeatedly, DNA damage can accumulate with aging, compromising the fidelity of gene transcription, accelerating cellular senescence, and raising the risk of cell death. Evidence of oxidative DNA damage in Lewy body disorders such as Parkinson's disease and dementia with Lewy bodies was originally reported decades ago, but the consequences of this aberration and the failure of DNA repair mechanisms are just beginning to be understood (Alam et al., 1997; Basu et al., 2015; Dent et al., 2022; Gonzalez-Hunt and Sanders, 2020; Kume et al., 2012; Lyras et al., 1998; Sanders et al., 2014; Schaser et al., 2019; Surguchev and Surguchov, 2017; Zhang et al., 1999). Lewy body disorders are defined by the aggregation and deposition of the abundant protein α-synuclein into hallmark inclusions within neuronal somata and processes (Attems et al., 2021; Goedert et al., 2013; Oliveira et al., 2021). Under physiological conditions, α-synuclein is enriched within synapses, but a fraction of the α-synuclein pool is also housed in the nucleus, where it plays a role in transcriptional regulation and is recruited to DNA damage sites to regulate genome repair (Dent et al., 2022; Garcia-Esparcia et al., 2015; Goncalves and Outeiro, 2013; Ma et al., 2014; Maroteaux et al., 1988; Paiva et al., 2017; Pavlou et al., 2017; Pinho et al., 2019; Schaser et al., 2019; Schell et al., 2009; Siddiqui et al., 2012; Surguchev and Surguchov, 2017; Surguchov, 2015; Zhou et al., 2013). Hence, the aggregation of α-synuclein in cytosolic Lewy bodies may divert this protein from the nucleus and synapse, leading to loss-of-function neurotoxicity [discussed by (Schaser et al., 2019)]. Conversely, when α-synuclein is aggregated and/or oxidized, it may also gain toxic endonuclease function when it associates with chromatin, thereby eliciting DNA strand breaks and activating the DNA damage response (Milanese et al., 2018; Rocha et al., 2018; Schaser et al., 2019; Tapias et al., 2017; Vasquez et al., 2017; Yoon et al., 2022).

Pathological phosphorylation of α-synuclein at the Serine 129 residue (pSer129) is an established marker of Lewy pathology (Anderson et al., 2006; Fujiwara et al., 2002) and can inhibit the DNA-binding and DNA-bending properties of α-synuclein (Dent et al., 2022). In addition, pathologic α-synuclein activates the DNA damage response protein poly(ADP-ribose) polymerase 1 (PARP1), and poly(ADP-ribose) (PAR) may accelerate the development of α-synucleinopathy (Kam et al., 2018). Indeed, patients with Parkinson's disease display elevated levels of PAR in the cerebrospinal fluid compared to controls (Kam et al., 2018), and dermal fibroblasts harvested from patients with Parkinson's disease display impairments in nucleotide excision repair (Sepe et al., 2016). Lewy inclusion-bearing neurons in the human amygdala also express the DNA damage response marker γH2AX (Schaser et al., 2019). *Ercc1* mutant mice with compromised nucleotide excision

repair display loss of nigrostriatal pathway markers and higher levels of pSer129 (Sepe et al., 2016). Thus, emerging evidence supports continued exploration of a link between α-synuclein and the integrity of the genome—a link that may play an underappreciated role in the onset and progression of Lewy body disorders.

Under conditions of sublethal oxidative DNA damage, DNA integrity can be restored by base excision repair (BER), the dominant DNA repair pathway in neurons (Barzilai et al., 2008; Fortini and Dogliotti, 2010). BER commences with the excision of a damaged base through glycosylase-mediated hydrolysis of the base-sugar bond. This generates a temporary apurinic/apyrimidinic (AP), or abasic site, prompting the abundant DNA repair enzyme, AP endonuclease 1 (APE1), to cleave the phosphodiester backbone 5' of the AP site, thereby creating a 3' OH group and a 5' deoxyribose phosphate residue (Li et al., 2011; Whitaker and Freudenthal, 2018). DNA polymerases then insert new nucleotides, and DNA ligases reunite the DNA strands. Also known as redox effector factor 1 (REF-1), APE1 serves manifold roles, including as a redox co-activator of transcription factors (*e.g.*, NFKB, HIF1α, AP-1, and p53), a regulator of intracellular reactive oxygen species, a processor of microRNAs, and determinant of RNA quality control (Antoniali et al., 2017; Barchiesi et al., 2021; Caston et al., 2021; Kim et al., 2010; Malfatti et al., 2021; Vascotto et al., 2009). APE1 expression is concentrated within the nuclear compartment, but it also functions in the cytoplasm and modulates inflammatory cascades (Baek et al., 2016; Choi et al., 2013; Di Maso et al., 2007; Lee et al., 2011; Mijit et al., 2021; Park et al., 2013; Tell et al., 2005). APE1 is controlled by changes in gene expression, post-translational modifications (*e.g.*, acetylation and phosphorylation), proteolytic cleavage, and subcellular translocation, and functional APE1 can be released from cells through exosomes (Fan et al., 2003; Lopez et al., 2021; Mangiapane et al., 2021; Thakur et al., 2015). Exosomal APE1 retains its ability to repair DNA and assumes p37 or p33 forms via proteasomal processing (Mangiapane et al., 2021). Recent studies further show that exosomal APE1 secretion from vascular endothelial cells is enhanced by 17ß-estradiol exposure (more so than by dihydrotestosterone) and that APE1 secretion is augmented upon 17ß-estradiol delivery to ovariectomized mice (Lee et al., 2021). In addition, APE1 expression in the cerebral cortex of ovariectomized mice is increased after exposure to 17ß-estradiol under hypoxic (but not normoxic) conditions (Dietrich et al., 2013), whereas APE1 expression in the uterus is decreased by 17ß-estradiol exposure (Dietrich et al., 2013). In individuals exposed to pesticides, APE1 polymorphisms have been linked to an increased risk of Parkinson's disease, and APE1 function may be blunted in the brains of Parkinson's disease subjects (Gencer et al., 2012; Huang et al., 2010; Sanders et al., 2014; Sanders et al., 2017). Preclinical evidence also supports the involvement of APE1 in MPTP-driven dopaminergic cell degeneration in male mice (Huang et al., 2010). Knockdown and overexpression studies conducted *in vitro* suggest that neuronal expression of APE1 is protective against oxidative challenges (Vasko et al., 2005). We have shown that APE1 overexpression *in vivo* alleviates stroke injury in male rats through its DNA repair function (Leak et al., 2015), whereas conditional APE1 knockout in adulthood aggravates stroke outcomes in male mice (Stetler et al., 2016). Given emerging connections between α-synuclein and DNA damage/repair, and evidence specifically favoring the pleiotropic nature of APE1, we commenced a broad investigation of

APE1 in the context of Lewy body disorders and biological sex, and centered our attention on the limbic system.

The limbic system is a broadly defined set of primordial brain structures in support of olfaction, memory, and emotional and autonomic regulation. Archetypal components of the limbic system reside along the border (*limbus*) of the cerebral hemispheres, including the amygdala and anterior olfactory nucleus (AON) (Murray, 2007; Soudry et al., 2011). The AON and amygdala develop intense α-synucleinopathy in Lewy body disorders (Beach et al., 2009a; Beach et al., 2009b; Braak et al., 2003; Pearce et al., 1995; Ubeda-Banon et al., 2010; Ubeda-Banon et al., 2013) and may participate in non-motor symptoms, such as anosmia, anxiety, anhedonia, and depression (Paxinos, 2015; Sorrentino et al., 2019; Stoyka et al., 2020). In order to model limbic Lewy-related pathology in the present study, we chose to infuse preformed fibrils into the rear of the mouse olfactory bulb (OB), which houses the bulbar extension of the rostral AON (Paxinos and Franklin, 2013). Fibril infusions into the OB elicit pSer129^{+} inclusions that are densest within the limbic rhinencephalon (Mason et al., 2016; Mason et al., 2019; Rey et al., 2018; Rey et al., 2016a; Rey et al., 2016b). Here, we leveraged the latter animal model to assess the potential relationship between α-synucleinopathy and APE1. Briefly, we sought to, **1**) test the impact of APE1 knockdown or pharmacological inhibition on α-synuclein^{+} inclusion formation and cell loss in primary hippocampal cultures, **2**) measure the effects of limbic-centered α-synucleinopathy and biological sex on APE1 expression and DNA excision/repair function *in vivo*, and **3**) examine APE1 expression in postmortem OB and amygdalar tissue extracts from men and women with Lewy body disorders.

2. Methods

Additional detailed methods, 19 figures, and two antibody tables are in the Supplemental Materials.

2.1. Preformed α-Synuclein Fibrils

Preformed fibrils were developed from recombinant, wildtype mouse α-synuclein using published protocols (Polinski et al., 2018; Volpicelli-Daley et al., 2014). Frozen aliquots of stock α-synuclein fibrils (5 mg/mL) were stored at −80°C. Ten microliters of thawed fibrils were placed in a sealed 0.5 mL tube, tightly wrapped with multiple layers of Parafilm, and sonicated continuously for one hour in an ultrasonic waterbath (Bransonic M1800, Branson Ultrasonics Corporation, Danbury, CT). The latter sonication protocol was previously found to enhance the density of limbic inclusions *in vivo* (Mason et al., 2016).

2.2 Animals and Surgeries

All procedures were approved by the Duquesne University Institutional Animal Care and Use Committee and in compliance with the *NIH Guide for the Care and Use of Laboratory Animals*. CD-1 mice were bred and housed in a 12:12 photoperiod with *ad libitum* access to food and water. The colony was regularly repopulated with breeders from external sources (*e.g.,* Charles River, Wilmington, MA) to prevent genetic drift. Sprague Dawley rats were

also purchased from Hilltop Lab Animals (Scottsdale, PA) at regular intervals to repopulate an in-house breeding colony for primary cultures.

For fibril infusions into the OB/AON, mice were anesthetized with 2-3% vaporized isoflurane and the skull was stabilized in a stereotaxic frame (Stoelting, Wood Dale, IL). Coordinates were initially based on Paxinos and Franklin's atlas (Paxinos and Franklin, 2013), but verified with blue dye injections, as CD-1 mice are bigger than the 26-30 g, 3-month-old C57/BLJ6 mice used in the atlas. The optimized OB/AON coordinates for CD-1 mice are, relative to Bregma, AP +4.0 mm, ML −1.0 mm, and DV −2.5 mm (from top of skull rather than dura mater). Animals were infused with a Hamilton syringe (80330, Hamilton, Reno, NV) attached to a motorized injection pump (Stoelting) at a rate of 0.25 μL/min. Infusions were followed by a four-minute rest period, prior to slow needle withdrawal. Animals were then administered 0.05 mg/kg buprenorphine subcutaneously and placed on a heating pad until recovery. Topical lidocaine was applied to the incision site for three days.

For mice or rats subjected to histological procedures (including the PANT assay), animals were anesthetized and perfused through the heart with 20 units/mL heparinized saline (50 mL for mice or 100 mL for rats), followed by 4% formaldehyde (100 mL for mice, 300-400 mL for rats) in 0.1 M phosphate buffer. Brains were removed and submerged in 4% formaldehyde for an additional 2-3 hours and then immersed in 30% sucrose in 10 mM PBS for at least 48 hours. A 1-in-5 (mice) or 1-in-6 (rats) series of 40-50 μm-thick brain sections was collected on a freezing sliding microtome (Model 860, Rankin, Holly, MI) and stored in cryoprotectant at −20°C. For biochemical assays, mice were anesthetized with isoflurane and euthanized by decapitation. Further details can be found below and in the Supplemental Materials.

2.3. Behavior Assessments

The buried food and wooden block olfactory tests were performed to measure olfactory function in male mice, as described (Lehmkuhl et al., 2014; Mason et al., 2019). First, the latency to find a peanut buried in clean corncob bedding was videotaped and measured by a blinded investigator two months following PBS or fibril infusions into the OB/AON. Second, five wooden blocks (1 cubic inch) were placed in all cages for one week to absorb murine odors. On the testing day (three months after PBS or fibril infusions in the OB/AON), mice were presented with four of these blocks from their own cages (familiar odor) plus one unfamiliar block in random order with novel odors from a different mouse cage or swabbed with vanilla, almond, or peppermint extract. The murine odor block test and the flavor extract tests were conducted for three trials each and results from these six trials were averaged. A blinded investigator viewed the videotapes and measured a) the latency until the snout made contact with the block, and b) time spent contacting the block harboring a novel, unfamiliar odor (flavor extracts and cage odors) *versus* a familiar-smelling block from their own cage.

To test anxiety-like aversion to open spaces (Frye et al., 2000), two, 5-minute trials were carried out in a 2 ft. × 2 ft. × 1.5 ft. (L × W × H) open field arena on consecutive days. The open field space was divided into a total of 16 squares (6 in. × 6 in.; 12 peripheral and 4

central squares). Each mouse began the trial at the center of the arena and was left to roam freely for 5 minutes without distractions. The walls and floor of the open field were cleaned with Quatricide (Pharmacal Research Labs, Waterbury, CT) between each trial. Two blinded observers recorded the number of rears and the number of central square entries for each mouse, while ANY-maze software was used to plot the animals' paths and assess the number of central square entries, distance traveled in meters (m), mean and max speeds (m/s), the number of immobile episodes (number of episodes during which the animal stopped traveling across the floor), and the time inactive in seconds (s) [total time with lack of any motion (traveling, grooming, rears, *etc.*)].

To further evaluate mood and anxiety, preference for sucrose-sweetened *versus* regular drinking water was assessed, as described previously (Gross and Pinhasov, 2016). Mice were individually housed for 24 hours with *ad libitum* access to food and water. Animals were pre-exposed to 2.5% sucrose for 2 hours to minimize neophobia. Preference for 1% sucrose water over regular drinking water as well as total liquid intake were then measured for 24 hours. Bottles were weighed prior to placement in the cage by a blinded investigator. Bottles were randomly assigned to separate sides of the cage. After 12 hours, the position of the bottles was switched to avoid confounding effects of side preference. At the end of the 24-hour period, animals were returned to their home cages and bottles were weighed again. Sucrose water preference was calculated as the percentage of total liquid intake attributed to the 1% sucrose solution using the following equation: [1% sucrose solution consumed in grams / (1% sucrose solution consumed + regular drinking water consumed in grams)] × 100. Total liquid intake was calculated using the following equation: [1% sucrose solution (g) + regular drinking water (g)] / body weight (g). All bottles were prepared one day before use and stored on their sides in the mouse room. Prior to the experiment, bottles were placed in empty cages to ensure no leakage.

2.4. PANT Labeling of Damaged DNA

DNA polymerase I-mediated biotin-dATP nick-translation (PANT) labeling was performed on free-floating brain sections, based on prior descriptions (Chen et al., 1997). Sections were removed from cryoprotectant and washed 3 times in 10 mM PBS for 5 minutes / wash. The tissue was then permeabilized in PBS with 1% Triton X-100 for 30 minutes and washed 3 times again in PBS. ThermoFisher Scientific's Endogenous Biotin-Blocking Kit (E-21390) was used to minimize interference of endogenous biotin. Tissue sections were incubated for 20 minutes with the streptavidin reagent (component A) and then with the biotin reagent (component B) for another 20 minutes, as per manufacturer directions. Each incubation was followed by one 5-minute PBS wash. Sections were incubated for ten minutes in PANT buffer containing 5 mM magnesium chloride (M1028, Sigma-Aldrich, St. Louis, MO), 10 mM 2-mercaptoethanol (31350010, Thermo Fisher Scientific, Pittsburgh, PA), and 20 μg/mL bovine serum albumin (BSA; A30075, RPI, Mt. Prospect, IL) in PBS. Next, tissue was incubated at 37 °C for one hour, protected from light, in the PANT reaction mixture containing dGTP, dCTP, and dTTP at 30 μM each, 1 μM dATP (dNTP Solution Set N0446S, New England BioLabs, Ipswich, MA), 29 μM biotinylated dATP (19524016, Thermo Fisher Scientific, Pittsburgh, PA) and 40 U/mL Escherichia coli DNA polymerase I (M0209S, New England BioLabs, Ipswich, MA) in PANT buffer. The PANT reaction was followed by three

PBS washes containing 0.5 mg/mL BSA for 5 minutes/wash. Sections were then incubated for one hour with the streptavidin, Alexa Fluor 546 conjugate (S11225, Thermo Fisher Scientific, Pittsburgh, PA) at a concentration of 10 μg/mL in PBS with 0.5 mg/mL BSA. Tissue was washed for 5 minutes in PBS and then exposed to the Hoechst 33258 reagent (bisBenzimide, 5 μg/mL; B1155, Sigma-Aldrich, St. Louis, MO) for 15 minutes. Sections were washed 3 times in PBS for 5 minutes/wash and mounted on glass Superfrost Plus Gold Microscope Slides (Fisher Scientific, Pittsburgh PA), dried, and coverslipped with Krystalon mounting media (64969, EMD Chemicals, Gibbstown NJ) or FluoroMount-G mounting medium (0100-01, SouthernBiotech, Birmingham, AL).

As a positive control, adjacent sections were treated for 5 minutes with 200 U/mL DNase I (90083, Thermo Fisher Scientific, Pittsburgh, PA) in 10 mM PBS at 37 °C following the abovementioned permeabilization step with Triton X-100. Brain sections were then washed 3 times in PBS for 5 minutes/wash prior to blocking endogenous biotin, and all subsequent steps were followed as outlined above.

2.5. GlycoSPOT and ExSySPOT assays

For assessments of DNA repair/excision activity, OB/AON tissues were weighed and quickly immersed in sterile DMEM (D6046, Sigma-Aldrich, St. Louis, MO) at room temperature. Tissues were then submerged in cell culture freezing media with dimethyl sulfoxide (DMSO; S-002-D, Sigma-Aldrich, St. Louis, MO) and stored at −80 °C or on dry ice until assay. Thawed tissues were washed once in ice-cold PBS, suspended in ice-cold buffer A [90 mM HEPES pH 7.8, 630 mM KCl, 2 mM EDTA pH 8.0, 20% glycerol, 0.3% Triton X-100, and 1 mM DTT] at 7.5 μL per mg of tissue and then disrupted and homogenized for 30 seconds (Qiagen TissueRuptor). The lysis was completed by two cycles of freezing/thawing in liquid nitrogen and at 4 °C, respectively. Ice-cold buffer B [45 mM HEPES pH 7.8, 0.25 mM EDTA pH 8.0, 2% glycerol, 1 mM DTT, 0.1 mM phenylmethylsulfonyl fluoride, 0.7× Protease Inhibitor Cocktail] at 4.35 μL per mg of tissue was subsequently added before a second round of freezing/thawing. Extracts were centrifuged for 10 minutes at 16,000 × *g* at 4 °C. The supernatant was recovered and protein concentrations were measured by the bicinchoninic acid Pierce Protein Assay Kit (23225, Fisher Scientific, Pittsburgh, PA).

DNA lesion cleavage and DNA lesion repair activity were assessed using the Glyco-SPOT and ExSy-SPOT assays (LXRepair), respectively, as published (Forestier et al., 2012; Millau et al., 2008; Pons et al., 2010; Prunier et al., 2012). A multiplexed oligonucleotide cleavage assay (Glyco-SPOT) was used to assess DNA lesion excision/cleavage of abasic sites paired with A (THF-A), hypoxanthine (Hx-T), 8-oxoguanine paired with C (8oxoG-C), thymine paired with G (T-G), ethenoadenine paired with T (EthA-T), A paired with 8oxoguanine (A-8oxoG), uracil paired with A (U-A), uracil paired with G (U-G), and thymine glycol paired with A (Tg-A). Briefly, each synthetically lesioned oligonucleotide (plus a lesion-free oligonucleotide) was labeled at its 3’ end with a fluorochrome and supported at two sites per well. Sample extracts were added to the wells (10 μg/mL protein concentration for all samples), and excision/cleavage of each lesion by specific enzymes in the extracts led to the release of the fluorescent labels. All samples were run in duplicate, and fluorescence

intensity measurements from two sample-free wells (excision buffer only) were used for normalization (100% fluorescence). Raw fluorescence intensities for each lesioned oligonucleotide were divided by fluorescence of the same lesioned oligonucleotide in the control wells without any sample. Percentage DNA lesion cleavage was then calculated using the following equation: [1 - (normalized fluorescence for each lesion / normalized fluorescence for lesion-free oligonucleotides) × 100].

The ExSy-SPOT assay was used to examine the repair of glycols, abasic sites (AbaS), pyrimidine dimers and (6-4) photoproducts (CPD-64), alkylated bases (Etheno), and 8-oxoguanine (8oxoG) by base excision and nucleotide excision repair-mediated incorporation of fluorescence-labeled nucleotide substrates into the repair of synthetically lesioned DNA plasmids immobilized on a biochip. A non-modified plasmid (control) was also immobilized in parallel. All samples were run in duplicate on two separate biochips (1 mg/mL protein concentration for each sample) and each plasmid was spotted at four locations per biochip. Quantified fluorescence was proportional to the ability of enzymes in the sample to repair each synthetic lesion. Raw fluorescence intensity values for repair of each lesion, obtained after subtraction of control plasmid fluorescence and fluorescence normalization as described in [63], are reported in Figures 8 and S18. In Figure S18G, repair of photoproducts by nucleotide excision repair is expressed relative to overall DNA repair activity, using the following equation: [(raw fluorescence intensity value for repair of each synthetic lesion / raw fluorescence for repair of all lesions) × 100]. Aside from raw data in Figure 8C and 8G, differential expression changes in DNA cleavage and DNA repair activity after fibril infusions are also expressed as the difference between individual fibril-infused animals and the mean of all PBS-infused animals, to illustrate sex-biased patterns in Figure S8B and S8F.

2.6. Statistical Analyses and Blinding

Experimental assessments (except the loading of samples onto gels for SDS-PAGE) were performed in a blinded manner, including imaging and behavior analyses. All graph types show every biological replicate as a colored dot. For *in vitro* studies, each blue dot denotes cells plated from one litter of mixed-sex pups (*i.e.,* the average of the triplicate wells). Data presented as bars with interleaved scatter plots show the mean with standard deviations. Heatmaps also display data as means, whereas violin and box plots illustrate the median and interquartile ranges. Single outliers were identified by the Grubb's test, but *all data are presented both with and without these statistical outliers*, as discussed in the Results or Figure Legends for panels S11A-B, S17A, and S17E-G. One or two-way ANOVAs were followed by the Bonferroni *post hoc* test (IBM SPSS Version 23, Armonk, NY). Two-tailed unpaired Student's *t* tests and two-tailed Pearson correlation analyses were conducted using GraphPad Prism (Version 9). Except where indicated, *t* tests were unpaired. The Kruskal Wallis, Mann-Whitney U, or Spearman's rank-order correlation analysis was used for non-normally distributed data. The two-tailed alpha was set at 0.05 for all analyses.

2.7. Study Approval

Human tissues were acquired postmortem via the Institutional Review Board (IRB)-approved repository at the National Institutes of Health NeuroBioBank and, upon discussion

with the head of our IRB, not subject to consideration for approval at Duquesne University. Only deidentified tissue samples were shipped to Duquesne. Protocols for each NeuroBioBank repository have been approved by respective IRBs. Further details on human tissues can be found in the Supplemental Materials, the NeuroBioBank online portal, and our prior work (Bhatia et al., 2021).

3. Results

3.1 Primary Neural Culture Model

Treatment of murine embryonic hippocampal cultures with preformed fibrils is an established paradigm for *in vitro* modeling of Lewy-related pathology (Polinski et al., 2018; Volpicelli-Daley et al., 2014). Here, we plated primary neural cultures harvested from the postnatal rat hippocampus and observed pSer129$^+$ structures after fibril exposure (Figure 1A, S1A-C). Perinuclear pSer129$^+$ structures were formed within the boundaries of MAP2$^+$ neuronal somata and threadlike structures were formed along β-tubulin III$^+$ processes (Figure S1B). Some inclusions were formed within nuclear boundaries (Figure S1B, top panel), consistent with prior work on the cytosolic as well as nuclear localization of α-synuclein, including the Ser129-phosphorylated form (Dent et al., 2022; Goncalves and Outeiro, 2013; Pinho et al., 2019; Schaser et al., 2019; Schell et al., 2009; Villar-Pique et al., 2016). As reported by Volpicelli-Daley and colleagues (Volpicelli-Daley et al., 2014), pSer129 inclusions were not solubilized by Triton X-100 added during fixation (Figure S2). For additional characterization of our postnatal rat neural culture models, please see our prior work (Crum et al., 2015; Heinemann et al., 2016; Posimo et al., 2014; Posimo et al., 2015) and consult Figures S1 and S3b in our recent report on fibril-induced pSer129$^+$ pathology in rat hippocampal cultures (Bhatia et al., 2021).

Previously, we showed that the fibrils do not lead to robust cell loss in our postnatal culture model (Bhatia et al., 2021), perhaps because our cultures contain a mixed population of neurons and astrocytes, as conceded in our prior reports (Bhatia et al., 2021; Crum et al., 2015; Heinemann et al., 2016; Posimo et al., 2015). Thus, we assessed the neuronal *versus* astrocyte distribution of APE1 in our rat hippocampal cultures. APE1 was expressed at high levels in nuclei of NeuN$^+$ neurons, but was also present in GFAP$^+$ astrocytes *in vitro* (arrows in Figure S3A), consistent with the rat hippocampus *in vivo* (Figure S3B-C) and with prior immunohistochemical studies (Dragunow, 1995). Given the observation that hippocampal APE1 is predominantly neuronal, but also evident in astrocytes, our mixed neuron/astroglia cultures from the rat hippocampus were appropriate for testing the *in vitro* impact of APE1 knockdown on α-synucleinopathy.

3.2. Loss of APE1 Expression Worsens α-Synucleinopathy in Vitro

We tested the role of APE1 in α-synucleinopathic inclusion formation by knocking down APE1 expression in primary hippocampal cultures with lentivirus constructs. Of seven APE1-shRNA constructs tested from two independent manufacturers, APE1 expression was only reduced by ~20-30% (Figures S4, 1B), whereas higher transducing units led to cell loss and detachment (not shown). Our difficulties with APE1 knockdown may reflect the essential nature of APE1 in postmitotic neurons and is consistent with the embryonic

lethality of knocking out the *Apex1* gene (Xanthoudakis et al., 1996). An unexpected increase in APE1 expression was observed with Dharmacon construct 2 (Figure S4B-C), consistent with the view that APE1 may be stress-reactive and involved in inflammatory signaling (Baek et al., 2016; Jedinak et al., 2011; Oliveira et al., 2022; Zaky et al., 2018). Origene lentivirus constructs did not raise APE1 levels, and sequences B, C, and D knocked down APE1 expression in fibril-treated cultures, as assessed *in situ* with the low-resolution/high-sensitivity In-Cell Western method (Posimo et al., 2014) and expressed as a fraction of DRAQ5$^+$ nuclear signal (Figure 1B). Further assessment of shRNA sequences C and D revealed no changes in cell counts or the average size of pSer129$^+$ inclusions compared to the non-targeting control sequence (Figure 1C-D). However, loss of APE1 expression increased the density of pSer129$^+$ inclusions in the fibril-treated groups (Figure 1E, S5), revealing a potential link between loss of APE1 expression and *in vitro* α-synucleinopathy.

Next, we treated primary hippocampal cultures with APE1 Inhibitor III [IC_{50} of 2 μM in prior work (Rai et al., 2012)]. No statistically significant changes in the number of Hoechst$^+$ or APE1$^+$ cells (Figure 1F-G) or average pSer129$^+$ inclusion sizes (Figure 1H) were noted. However, neurons treated with fibrils in the presence of 2 μM APE1 Inhibitor III displayed denser pSer129$^+$ inclusions than DMSO-treated control cells (Figure 1I-J, S6A-B). Lack of concentration-dependency of the effect on inclusion densities was unexpected, but higher concentrations of APE1 Inhibitor III were severely toxic and led to cell detachment (not shown). We only observed a statistical trend towards an increase in the density of abasic sites with 2 μM of APE1 Inhibitor III (two-tailed $p = 0.0587$; Figure S6C). APE1 is responsible for >95% of total abasic site activity (Chen et al., 1991; Li and Wilson, 2014). Thus, lack of a robust effect on abasic sites at non-lethal concentrations of APE1 Inhibitor III may explain the modest average increase in inclusion counts in Figure 1I. Subcellular localization of pSer129$^+$ inclusions was not affected by the application of APE1 Inhibitor III in fibril-treated cultures (Figure 1J, S1D). In contrast to the APE1 inhibitor III results, a selective inhibitor of the redox function of APE1, E3330 (Domenis et al., 2014), did not exert statistically significant effects on inclusion numbers compared to the DMSO vehicle control group (Figure S7). As no assay for APE1 redox function was completed in this *in vitro* model, we do not rule out critical functions for the redox roles of APE1. Nonetheless, interfering with APE1 increases (likely indirectly) pSer129$^+$ inclusions within primary hippocampal neurons *in vitro*.

3.3. Biological Sex Modifies the Impact of α-Synucleinopathy on APE1 Expression in Mice and Humans

We assessed changes in the expression of APE1 in response to α-synuclein fibril infusions in male and female mice. Fibril or PBS infusions were targeted to the OB/AON to generate α-synucleinopathy in the limbic system without robust cell loss, as detailed in our previous work (Bhatia et al., 2021; Mason et al., 2016; Mason et al., 2019). When we commenced our work on the preformed fibril model, we used unsonicated monomeric α-synuclein as well as PBS as negative controls (Nouraei and Leak, unpublished). However, we observed some pSer129$^+$ inclusions in the monomer groups. The presence of sparse inclusions models incidental Lewy body disease, which is believed to progress into a bona fide Lewy body disorder (Beach et al., 2009a; Beach et al., 2008; Dickson et al., 2008; Iacono et al., 2015).

Others report similar *in vivo* observations with monomeric α-synuclein (Patterson et al., 2019; Paumier et al., 2015). Hence, we used PBS to mimic truly unaffected controls (also see Discussion).

Six months following PBS or fibril infusions, mouse brains were sectioned in the sagittal plane and infrared APE1 immunostaining was quantified on 16 bit-depth grayscale images in order to delineate cytoarchitectural boundaries with more anatomical precision than is afforded with tissue dissections (Figure 2A, regions of interest sketched in Figure 2B). A blinded observer divided the $APE1^{+}$ signal in the regions of interest by the area of the traced outline, as described (Nouraei et al., 2018), to control for atrophic changes in response to fibril infusions or potential sex differences in brain size. Heatmaps of the average APE1 signal in traces of each brain region revealed high APE1 expression in the OB of male and female mice (Figure 2A-D). In contrast, APE1 expression in the more vulnerable AON was low compared to other limbic regions (Figure 2A-D; high exposures with low contrast were used to visualize virtually all signal and background in Figure S8A).

Next, we assessed the impact of sex and fibril exposure on global APE1 expression in the prosencephalon and brainstem. No net changes in overall brain size were noted (Figure S8B)—supporting use of the same stereotaxic coordinates for both sexes. Fibril infusions in the OB/AON elicited a mild but unexpectedly global loss of APE1 expression in male mouse brains (Figure 2E). In contrast, females responded to fibril infusions with a modest increase in net APE1 expression levels. In addition, PBS-infused females displayed lower APE1 levels than PBS-infused males (Figure 2E). A statistical interaction between biological sex and the disease model was thus noted in the measurements of brain APE1 (Figure 2E). When expressed as the degree of change elicited by fibril infusions (the difference between fibril-infused animals and the mean of all PBS-infused animals), the changes in global expression levels of APE1 after fibril exposure were negative for males, but positive for females (Figure 2F), suggesting divergent effects of fibrils based on biological sex.

We tested if the sex differences in APE1 protein in the fibril-treated brain were reflected in mRNA, and a trend towards a statistical interaction between biological sex and disease state was observed by RT-qPCR ($p = 0.052$; Figure 2G). When expressed as the difference between fibril and PBS-infused animals, APE1 mRNA levels in the diseased brain were again higher in female mice than male mice, whether nonparametric or parametric tests were applied (Figure 2H; $p = 0.008$ for two-tailed Mann-Whitney U and $p = 0.010$ for two-tailed unpaired *t* test; passed Kolmogorov-Smirnov but failed Shapiro-Wilk normality tests). Thus, sex-biased effects on *Apex1* gene expression are modest, but nonetheless evident at the level of murine protein and mRNA.

In the mouse cerebellum, an interaction between sex and experimentally-induced disease was noted (Figure S8C), as well as fibril-induced net loss of APE1 in males *versus* an increase in females (Figure S8D). The cerebellum lies at a considerable distance from the site of fibril infusions, highlighting the unexpectedly far-reaching sex-dependent response of APE1 to OB/AON fibril infusions.

In the mouse AON, fibril infusions elicited loss of APE1 expression in males and an increase in females (Figure 2I-J). In addition, PBS-infused females displayed lower APE1 levels in the AON than males. There were no changes in the size of the AON (Figure S8F). The mouse OB displayed higher APE1 levels in fibril-infused females than males (Figure 2K-L). A statistical interaction between sex and disease was observed for APE1 expression in the mouse AON as well as OB. The OB was slightly atrophied six months after fibril infusions in male but not female mice (Figure 2M), which seems important in light of atrophy of the human OB in subjects with Parkinson's disease (Li et al., 2016).

Tissue samples from the OB of deceased male and female control subjects and subjects diagnosed with various Lewy body disorders were acquired through NIH NeuroBioBank from UCLA and subsequently also from the University of Miami. The demographics of these cohorts have been published and are available online in the NeuroBioBank portal [see Table S3 in (Bhatia et al., 2021)]. There were no group differences in age at death or postmortem interval [see Figure 8a-b in (Bhatia et al., 2021)]. We performed bulk RNA sequencing on the UCLA samples (Miner *et al.,* in progress; see Supplemental Methods) and mined those data *a priori* for *APEX1* gene expression. As predicted, the whole-transcriptome analyses did not pinpoint the *APEX1* gene as highly altered in expression levels across groups after false-discovery rate adjustments. Rather, changes in *APEX1* transcripts per million (TPM) were modest when analyzed *a priori* by two-way ANOVA (Figure 2N) or *t* test (Figure 2O). Consistent with the transcriptomics, immunoblotting tissues from UCLA and University of Miami cohorts demonstrated slightly higher APE1 expression in the OB of diseased women compared to diseased men (Figure 2P). Antibody specificity and the dynamic linear range of the assay had been prevalidated on human tissues (Figure S9). A brighter version of the immunoblot of Figure 2R is included in Figure S10. A statistical trend towards an interaction between sex and disease was noted for human APE1 expression (Figure 2P). Control female human subjects did not display basally lower APE1 expression than control male subjects, *but this was also not the case for the mouse OB* (compare PBS mice in **2K** with control subjects in **2P**).

When expressed as the difference between diseased and control groups, average changes in OB expression of APE1 were negative for men and positive for women (Figure 2Q)—as observed for our murine model. Semi-quantitative immunoblotting patterns in Figure 2P-R were correlated with immunoblotting patterns on the same samples with a different, prevalidated antibody against APE1 (NB100-101, Novus; Pearson $r = 0.6874$; two-tailed $p = 0.0135$; see Figure S9 for testing of both antibodies on human samples). No correlations between the postmortem intervals and APE1 expression were observed (Pearson $r = -0.2046$; two-tailed $p = 0.3161$).

APEX1 mRNA and APE1 protein levels showed a trend toward a linear association in the 12 OB samples from UCLA (Pearson $r = 0.5352$, two-tailed $p = 0.0730$) and a statistically significant linear correlation in the diseased UCLA samples (Pearson $r = 0.9541$, two-tailed $p = 0.0031$), but the n of 6 for RNA-seq on the diseased samples from UCLA was relatively low.

Given that our animal model mimics limbic-centered Lewy body disease, we tested the impact of sex and α-synucleinopathy on APE1 protein expression in the mouse and human amygdala. Starting with mice, we observed lower amygdalar APE1 expression in PBS-infused females than males, as well as an interaction between sex and disease (Figure 3A-B). Fibril infusions elicited a slight decrease in mouse amygdalar size—in males only (Figure 3C)—as noted above for the OB. Of note, Harding *et al.* reported a ~20% loss of *total volume* of the human amygdala in Parkinson's disease (mostly male subjects), which they attributed to loss of volume and neuron numbers (by stereological assessment) within the 'corticomedial' amygdala nucleus, which is heavily connected to olfactory structures (Harding et al., 2002). We have shown that pSer129 or retrograde tracer label is often concentrated within the posteromedial cortical amygdala [PMCo according to Paxinos (Paxinos and Franklin, 2013)] after injections of preformed fibrils or FluoroGold, respectively, into the mouse OB/AON (Mason et al., 2016; Mason et al., 2019). Other regions, such as the amygdalopiriform transition area are also affected. However, when the caudoputamen is infused with fibrils, Stoyka and colleagues report pSer129^{+} and proteinase K-resistant inclusions in the central and basolateral amygdalae (Stoyka et al., 2020). Thus, the topography of amygdalar inclusions vary with the zone of fibril uptake, as would be expected from a standard tract-tracing study.

Western blotting was used to measure APE1 expression in postmortem samples of the human amygdala. The combined cohorts displayed higher APE1 expression in diseased women compared to diseased men—whether nonparametric or parametric ANOVA testing was employed (Figures 3D-F, S10; one Grubb's outlier shown in the nonparametric test of Figure 3D was not included in the parametric tests on the same data shown in Figure S11A-B, as the distribution would then have been non-Gaussian). These semi-quantitative immunoblotting patterns were also correlated with those of the other prevalidated antibody against APE1 run on the same samples (NB100-101, Novus; Pearson r=0.7063; two-tailed p=0.0129). For boundaries of the human amygdalar dissections, consult Figure S11C. No correlations of APE1 expression and postmortem interval were observed in the amygdala samples (Pearson $r = -0.07253$; two-tailed $p = 0.7248$).

For the topographical extent of pSer129^{+} pathology, please consult our prior work, where we reporting not finding inclusions within the boundaries of the substantia nigra, pars compacta and only occasional inclusions within the ventral tegmental area (Mason et al., 2016; Mason et al., 2019). There were also few inclusions in the caudoputamen, but denser inclusions in the nucleus accumbens in some mice [Figure 10 of (Mason et al., 2019) and Table S2 of (Mason et al., 2016)]. These observations may be important in light of the role of the nigrostriatal projection to the caudoputamen in movement permissiveness and the role of the mesolimbic projection to the accumbens in reward-seeking limbic behaviors (Gardner, 2011; Humphries and Prescott, 2010). In the accumbens as well as caudoputamen, PBS-infused females exhibited lower APE1 levels than males, and an interaction between sex and disease was noted (Figure 3G-H, S12A). Furthermore, fibril-infused female mice displayed higher APE1 expression in the accumbens and caudoputamen than male counterparts (Figure 3I, S12B). The accumbens of male mice shrunk slightly after fibril infusions (Figure 3J), whereas the caudoputamen hypertrophied slightly in this group (Figure S12C). In the accumbens, female but not male mice responded to fibril infusions with an increase in the

density of APE1$^+$ cells, which could not be explained by parallel changes in NeuN$^+$ neuron densities (Figure 3K, L). In addition, PBS and fibril-infused females displayed lower APE1$^+$ cell densities within the caudoputamen compared to male counterparts (Figure S12D-E, high exposures with low contrast were used to visualize virtually all signal and background in S12F).

Measurements of APE1 were not possible in the ventral tegmental area due to loss of tissue along the bisected midline. However, in the substantia nigra, male mice responded to fibril infusions with a decrease in APE1 while females showed an increase, with interactions between sex and disease (Figure S8G-H). For the sake of completeness, additional limbic regions are quantified in Figure S13. The collective data reveal that, in some—*but not all*—brain regions, female mice with experimental Lewy body disease displayed higher APE1 expression than diseased male counterparts, a sex-dimorphic pattern that translated to the human OB and amygdala. In other words, we did not find higher average APE1 levels in fibril-infused males compared to fibril-infused females in any brain region.

3.4. Fibril Infusions do not Severely Damage DNA in Limbic Structures, Unlike 6-OHDA Infusions in the Striatum

We sought to determine the extent of DNA damage, as a function of fibril exposure and sex, with DNA polymerase I-mediated biotin-dATP nick-translation (PANT) labeling of single-stranded DNA. Two independent positive controls were employed. First, we used the enzyme DNase I, which leaves behind single and double-stranded DNA breaks when applied briefly to *ex vivo* tissue sections (Figure 4A). As the second positive control, PANT labeling was conducted in the substantia nigra after 6-hydroxydopamine (6-OHDA) infusions in the striatum *in vivo* (Figure 4B). 6-OHDA elicits oxidative stress and damages DNA (Bernstein et al., 2011), and infusions of 4 μg 6-OHDA centered in the striatum kill nearly 50% of nigrostriatal projection neurons in our hands, as we confirmed via *in vivo* transport of the retrograde tracer FluoroGold [Figure 4 in (Nouraei et al., 2016)]. Unexpectedly, mice infused with 4 μg 6-OHDA in the striatum displayed globally high PANT label compared to vehicle-infused mice (Figure 4B). These findings suggest that the traumatic impact of striatal 6-OHDA infusions may not be limited to the nigrostriatal pathway. Both positive controls point to the success of the PANT method in recognizing DNA damage, but no cellular PANT labeling was observed within the brains of fibril-infused male or female mice, including at the site of the infusion in the rostral bulge of the AON into the OB (Figure 4C-E). Similarly, neither sex nor disease modified the frequency of apurinic/apyrimidinic sites in DNA extracts from the piriform cortex (Figure 4F), a brain region that harbors massive inclusion numbers following OB/AON infusions (Mason et al., 2016; Mason et al., 2019).

3.5. Oxidative Stress May Contribute to the Mild Impact of α-Synucleinopathy on APE1 Expression

Given the evidence of robust DNA damage after 6-OHDA infusions in Figure 4B, we tested if this form of severe oxidative stress can also affect APE1 expression. Colocalization of APE1 and tyrosine hydroxylase in the substantia nigra, pars compacta, is depicted in Figure 5A, confirming its expression in dopaminergic as well as nondopaminergic neurons of the

ventral mesencephalon, but not showing net loss of APE1 with 6-OHDA exposure. Rather, an *increase* of APE1 was observed in the ipsilateral and contralateral substantia nigra and striatum after unilateral exposure to 6-OHDA (Figure 5B-F). In addition, the increase in APE1 expression in response to striatal 6-OHDA infusions was not limited to the ventral midbrain or striatum. Instead, a global rise in APE1 expression levels was noted in response to 6-OHDA exposure (Figure 5G-I), consistent with the expanse of PANT labeling in Figure 4B.

Results collected thus far suggested that severe oxidative stress in the striatum damages DNA and raises APE1 expression in the brains of male mice, but that OB/AON fibril infusions increase neither abasic sites nor PANT labeling in the brains of either sex. On the other hand, fibril exposure might elicit a different type of oxidative stress than the rapid metabolism of 6-OHDA, and this may be associated with modest loss of APE1 expression in males and *subtle* oxidative damage to DNA, perhaps below the threshold of current detection methods. To test this idea at a functional level—without having to resort to potentially insensitive detection methods for oxidative DNA damage—we evaluated the impact of the antioxidant N-acetylcysteine on fibril-mediated loss of APE1 expression in male mice. N-acetylcysteine is widely used to temper oxidative stress and has been shown to reduce α-synuclein pathology in male mice when administered orally (Clark et al., 2010; Ghosh et al., 2021). Thus, N-acetylcysteine was administered in food for three months to male mice infused with fibrils or PBS in the OB/AON. $pSer129^{+}$ inclusion counts in the AON were increased by fibril infusions in mice fed a regular diet, but not in mice placed on the N-acetylcysteine diet (Figure 6A-B). However, this effect was not uniform across the brain, even including the nearby piriform cortex, and the variance in fibril-induced inclusion densities was high (Figure 6A, C), as reported in our prior work (Bhatia et al., 2021; Mason et al., 2016; Mason et al., 2019; Nouraei et al., 2018) and as shown in the additional photomontages of Figures S14-S15. Nonetheless, fibril infusions elicited a mild decrease in APE1 expression in male mice fed a regular diet, globally, as well as within the AON (Figure 6D-F), again demonstrating modest effects of fibril-mediated proteinopathic stress on APE1 expression—in an independent animal cohort. Mice on the N-acetylcysteine diet displayed unexpectedly lower APE1 levels than mice on the control diet in the PBS groups; we believe this suggests that basal oxidative tone under physiological conditions (*e.g.*, from mitochondrial respiration) holds APE1 expression at slightly higher levels than after antioxidant supplementation. Thus, oxidative tone can place tension on enzymes with a redox function, such as APE1 (Li and Wilson, 2014; Tell et al., 2009; Thakur et al., 2015).

In contrast to control dietary conditions, APE1 expression was not lowered by fibril exposure in the groups fed N-acetylcysteine (Figure 6E-F). There was no impact of either independent variable (sex or disease factor) on body weight or daily food consumption (Figure 6G-H). Together, these findings imply that oxidative stress influences the fibril-induced loss of limbic and global APE1 expression in males, but that 6-OHDA-mediated severe oxidative stress, which kills dopaminergic neurons and causes widespread DNA damage, exerts the opposite effects on APE1 expression.

3.6. Biological Sex Modifies the Impact of α-Synucleinopathy on Neurological Function

Our prior work showed that fibril infusions in the OB/AON hindered the ability of male mice to locate buried food (Mason et al., 2019), which we verified in an independent cohort of animals (Figure S16), but we had not yet tested anxiety-like behaviors and anhedonia, which are closely related to limbic function. Thus, we performed the sucrose preference test for hedonic-like motivation and the open field test to measure avoidance of the central squares. For these assessments, we used the cohort of animals that had been designated for the abasic site assay, three months after bilateral fibril infusions in the OB/AON (timeline in Figure 7A). In males, fibril infusions elicited a decrease in preference for sucrose water over regular water (Figure 7B), highlighting a potential reduction in hedonic motivation. Baseline consumption of sucrose water in both PBS and fibril-infused females was similar to that of diseased males (Figure 7B). In females, fibrils elicited an increase in total liquid intake, and fibril-infused female mice drank more liquid compared to fibril-infused males (Figure 7C), a possible sign of anxiety (Hew-Butler et al., 2019). An interaction between sex and disease was identified for total liquid intake (Figure 7C).

Two independent, blinded observers and the ANY-maze behavioral tracking software were used to record the number of times each mouse entered the center of the open field. Across two trials in the open arena, fibril exposure elicited a decrease in the average number of central square entries in males only, and PBS-infused females made fewer entries into the central squares than PBS-infused males (Figure 7D-G). The inter-rater reliability across the two blinded investigators and ANY-maze measurements is shown in Figure 7H.

The open field test is used to simultaneously assess motor activity, mood, and anxiety-related aversion to open spaces (Frye et al., 2000), and locomotor activity levels are reported here because they can also influence how many times the rodent crosses the lines between squares. In males, fibril infusions decreased the number of rears and distance traveled, and increased immobile episodes (Figure 7I-K). Sex-biased patterns were observed for additional open field measures, including max speed, mean speed, and time spent inactive (Figure S17A-C). Unlike male mice, females responded to fibril infusions with an increase in maximum speed during the open field trials, but only when not considering the impact of one Grubb's outlier (see Figure S17A). PBS-infused female mice displayed fewer rears and more immobile episodes than PBS-infused male mice (Figure 7I, K), suggestive of greater *baseline* anxiety in females, consistent with clinical reports (Gater et al., 1998).

The number of rears in the open field test was positively correlated with the number of central square entries and inversely correlated with the number of immobile episodes (Figure 7L-M), suggesting that greater locomotion was indeed associated with less anxiety-like behavior in this animal cohort. A negative correlation of abasic sites with the number of rears and entries into the central squares of an open field was noted, but only in female mice, whether the data were analyzed with nonparametric or parametric testing (Figure S17D-G). Altogether, the preponderance of measures reveals greater behavioral impacts of α-synuclein fibril infusions in male mice compared to age-matched females, but females may differ in some limbic-related neurological traits from males at baseline.

3.6. Biological Sex Modifies the Impact of α-Synucleinopathy on DNA Repair Activity

We have not observed evidence of DNA damage in our model of olfactory-seeded limbic pathology. Nonetheless, the global, sex-dependent changes in *Apex1* gene expression and APE1 protein expression noted in Figure 2 hint that DNA damage/repair pathways might be subtly affected by fibril exposure in females, leading to potentially compensatory upregulation of APE1 in the fibril-challenged female sex. To study this possibility further, we assessed *functional* changes in DNA repair activity in tissue extracts of the male and female OB/AON in response to α-synuclein fibril infusions, with the following tools: 1) the Glyco-SPOT assay for excision of synthetic DNA lesions, and 2) the ExSy-SPOT assay for incorporation of nucleotide substrates to lesioned DNA plasmids immobilized on a biochip. The initial construction of the biochips and assay specificity have been discussed (Millau et al., 2008; Sauvaigo et al., 2004).

A heatmap summarizing the Glyco-SPOT assay for DNA lesion excision is shown in Figure 8A and DNA cleavage is displayed as the difference between fibril and PBS-infused mice in Figure 8B. Male mice displayed greater excision of multiple DNA lesions when challenged with fibrils compared to females, including hypoxanthine-thymine (Hx-T), 8-oxoguanine-cytosine (8oxoG-C), thymine-guanine (T-G), and uracil-adenine (U-A) lesions, which are repaired by the enzymes N-methylpurine DNA glycosylase (MPG), 8-oxoguanine glycosylase (OGG1), thymine-DNA glycosylase (TDG), and uracil-DNA glycosylase/single-strand selective monofunctional uracil-DNA glycosylase 1 (UDG/SMUG1), respectively (Figure 8B) (Krokan and Bjoras, 2013; Montaldo et al., 2019). Increased excision of DNA lesions in male fibril-exposed samples are also shown in Figure 8C for Hx-T, and in Figure S18A-B for A-8oxoG and 8oxoG-C cleavage.

The same tissues were subjected to the ExSy-SPOT assay (Figure 8E-H), which measures the ability of enzymes in tissue extracts to eliminate synthetic DNA lesions on the biochips, and then to use the undamaged complementary strand as a template for DNA synthesis (Sancar, 1994). DNA repair activity is shown as the difference between fibril and PBS-infused mice in Figure 8F. Female mice tended to display more robust fibril-induced DNA repair activity, including repair of glycols, abasic sites, photoproducts, and 8oxoG. Examples of the increased repair of DNA lesions in female fibril-exposed samples are shown in Figure S18C-G and abasic site repair levels are shown in Figure 8G. As noted above, APE1 is responsible for >95% of total abasic site activity (Chen et al., 1991; Li and Wilson, 2014).

Finally, we verified that excision or repair activity for each lesion was correlated with excision or repair of the other lesion types. Correlation matrices displayed as heatmaps reveal correlations across cleavage activities in the Glyco-SPOT assay and correlations across DNA repair pathways in the ExSy-SPOT assay (Figures 8D, 8H, and S19). In general, the ExSy-SPOT data displayed greater internal consistency. These data demonstrate that animals with high cleavage or repair activity of one type of lesion also tended to display high cleavage or repair activity of a different type of lesion, supporting the reliability of the functionalized assays on a biochip.

4. Discussion

Women have a lower risk of developing Lewy body disorders than men (Abraham et al., 2019; Beach et al., 2009a; Nelson et al., 2010) and there may be less microgliosis and neurodegeneration in the OB of female patients with Parkinson's disease compared to male counterparts (Flores-Cuadrado et al., 2021). However, conflicts on human sex differences have arisen in the literature on Lewy body disorders, perhaps due to a paucity of studies on early, drug-naïve patients (Picillo and Fasano, 2015). On average, women have slightly better smell but greater risks of developing anxiety and depression compared to men, including in *de novo*, drug-naive female Parkinson's patients (Abraham et al., 2019; Broen et al., 2018; Khedr et al., 2020; Liu et al., 2015; Sorokowski et al., 2019). *De novo* female patients with Parkinson's disease also display better cognition and less white matter connectivity disruption in the basal ganglia, amygdala, hippocampus, and thalamus than male patients (Liu et al., 2015; Tremblay et al., 2020). Although drug-naïve female Parkinson's patients display the same rate of deterioration as their male counterparts, they also have a later disease onset and higher striatal [^{123}I]FP-CIT binding of the dopamine transporter (Haaxma et al., 2007). On the other hand, recent studies demonstrate lower α-synuclein levels in the cerebrospinal fluid and more severe Lewy pathology scores in the frontal cortices, amygdala, and locus coeruleus of women (Iannuzzelli et al., 2020; van de Beek et al., 2020). Thus, the interaction between Lewy body disease and biological sex may be influenced not only by medication and gonadal hormone status (*e.g.*, number of years after menopause), the function of sex-specific genes such as Y-chromosome gene *Sex-determining Region Y* (Lee et al., 2019), brain region of interest (*e.g.*, heavier cortical involvement in dementia with Lewy bodies than in Parkinson's disease), but also coexisting tau, ß-amyloid, and other age-related pathologies.

Sex differences in the risk of developing Lewy body disorders may be genetic as well as environmental in origin, as older men may have suffered greater lifetime exposures to industrial toxicants linked to a higher probability of developing these diseases (Tanner et al., 2014). Notably, recent studies by De Miranda and colleagues suggest that rotenone-mediated destruction of the nigrostriatal pathway requires higher doses in female compared to male rats (De Miranda et al., 2019; De Miranda and Greenamyre, 2019; Goldman and Tanner, 2019). One advantage of animal research is that laboratory animals live under tightly controlled environmental conditions and can be injected in parallel with the same fibril preparation and dose at the same age (as in the present study). Hence, variations observed in male *versus* female laboratory mice are more likely to originate in biological differences. The present data could thus be interpreted to suggest that APE1 expression and DNA excision/repair activities are regulated by biological sex under conditions of α-synucleinopathic disease. Although some of the effect sizes are modest, the size of a biological effect *per se* does not necessarily reflect the degree of its importance to organismal fitness and survival or even its potential for translatability to humans. This is particularly true of expression changes in proteins with indispensable functions—such as base excision repair of the genome.

The main interpretations of our data are as follows. First, baseline APE1 expression in the murine brain is highest in the OB. Intense APE1 expression in the OB of both sexes

may reflect the proximity of the OB to the external environment and, therefore, greater likelihood of exposure to inhaled, DNA-damaging toxicants. Second, APE1 expression was higher in fibril-infused females than fibril-infused males, in a number of limbic and extralimbic brain regions. Although biological sex differences were not evident in every brain region, the responses of APE1 to fibril infusions extended into some regions distant from the infusion site, including areas with minimal to no α-synucleinopathic inclusion load in our model [*e.g.,* cerebellum, dorsal striatum (Mason et al., 2016; Mason et al., 2019)]. In this context, leveraging an animal model with circumscribed, limbic-centered pathology was fitting. Third, the sex-biased pattern first observed in mice translated to the OB and amygdalar tissues of women *versus* men with Lewy body disorders. These findings suggest that challenges to cytosolic protein homeostasis (proteostasis) can impact the state of genomic quality control measures, with sex-opposing patterns in a number of brain structures.

Fourth, modest loss of APE1 expression in primary hippocampal cultures by shRNA-mediated knockdown or pharmacological inhibition of its DNA repair function amplified the formation of inclusions harboring pathologically phosphorylated α-synuclein. These findings suggest that interfering with DNA repair capacities does intrude upon cytosolic protein quality control and *vice versa*, although the biochemical mechanisms may be indirect. Fifth, APE1 expression in males was influenced by oxidative stress levels *in vivo*, as noted by feeding mice chow with or without N-acetylcysteine for three months. Although N-acetylcysteine has a number of cellular effects, several studies corroborate the antioxidant potential of this thiol-repletion agent and its efficacy against α-synucleinopathy *in vivo* (Berman et al., 2011; Clark et al., 2010; Ghosh et al., 2021). N-acetylcysteine is a membrane-permeable cysteine precursor and crosses the blood-brain barrier in both rodents and humans (Farr et al., 2003; Katz et al., 2015). Katz *et al.* observed that oral doses ranging from 7 to 70 mg/kg (we used 200 mg/kg) lead to dose-dependent increases in N-acetylcysteine concentration (up to ~10 micromolar) within the cerebrospinal fluid (Katz et al., 2015). Oral doses of 7.5 mg/kg N-acetylcysteine have been shown to normalize neuronal glutathione content and antioxidant capacity in *EAAC1*$^{-/-}$ rodents in a buthionine sulfoximine-sensitive fashion [see Figure 2B in (Reyes et al., 2016)]. In healthy controls as well as patients with Gaucher's or Parkinson's disease, N-acetylcysteine has been shown to increase blood and brain concentrations of glutathione (Holmay et al., 2013). Finally, Milanese *et al.* have also demonstrated *in vitro* that N-acetylcysteine diminishes the formation of yH2AX^{+} foci in preformed fibril-treated SH-SY5Y cells (Milanese et al., 2018).

It is important to note that male mice were not refractory to upregulation of APE1, as acute, severe oxidative stress induced by infusions of 6-OHDA resulted in robust and global increases in APE1 in the male mouse brain. 6-OHDA may diffuse across the CNS via the interstitial fluid, even when delivered into striatal parenchyma, as it is relatively small and hydrophilic. In the past, investigators have infused 6-OHDA into the cerebrospinal fluid of the rat brain to lesion various catecholaminergic cell clusters [examples in (Commins et al., 1989; Gordon et al., 1985; Harsing and Zigmond, 1996; Keefe et al., 1990; Sadakierska-Chudy et al., 2010)]. At neutral pH, 6-OHDA breaks down into dopamine quinones and hydrogen peroxide, which could enter cells without reliance on the dopamine

transporter and damage DNA (Cohen and Heikkila, 1974; Krohn et al., 2007; Przedborski and Ischiropoulos, 2005; Valverde et al., 2018). Thus, our observations reveal that the impact of striatal exposure to the 6-OHDA toxicant is not specific to catecholaminergic cells, and that changes in APE1 are not inescapably small in effect size. Rather, the nature of the proteostatic/redox challenge determines the size *and direction* of the response in APE1.

In our hands, sex-dependent changes in APE1 expression in the brains of fibril-exposed mice were not associated with observable DNA damage, as measured by the ARP assay for abasic sites and PANT labeling for DNA strand breaks. However, according to two functional assays for DNA cleavage/repair activity, OB/AON tissue extracts from male mice displayed greater excision of several types of synthetic DNA lesions following *in vivo* fibril infusions, whereas female mice displayed greater repair of synthetic DNA lesions upon fibril exposure. It is possible that fibril exposure rapidly increases oxidative stress levels (independent of longer-term inclusion formation) and thereby drives DNA damage that is enzymatically repaired over time. Thus, subtle losses in genomic integrity following fibril infusions (perhaps at earlier survival timepoints than assessed here) may have induced compensatory responses (observed in DNA repair data of Figure 8) by the time the PANT and ARP assays were conducted. Hence, we do not rule out greater damage to the female genome under diseased conditions. Indeed, preliminary data of ours suggest higher levels of 4-hydroxynonenal-modified proteins in the OB of diseased women and fibril-infused female mice compared to males (Miner and Leak, in progress). Accordingly, female patients with Parkinson's disease display greater serum concentrations of 8-hydroxy-2'-deoxyguanosine/8-hydroxyguanosine compared to their male counterparts (Kikuchi et al., 2002). Thus, for those (fewer) women who do eventually succumb to Lewy body diseases, APE1 levels may be higher than in diseased men precisely because their genomes display greater oxidative damage. Prior studies indicated that biological sex does not influence baseline APE1 expression in lung cancer (Gu et al., 2013; Lu et al., 2018) and that the development of some types of cancer in patients with APE1 polymorphisms does not differ by sex (Lo et al., 2009). On the other hand, clinical studies hint at higher APE1 activity in women compared to men, in peripheral blood mononuclear cells (Sevilya et al., 2015) and in brain tumors (Bobola et al., 2005). Furthermore, women with a specific allelic variant of APE1 are at increased risk for colorectal cancer (Lai et al., 2016). As mentioned above, APE1 secretion from endothelia and APE1 expression in the hypoxic cerebral cortex are raised after 17ß-estradiol exposure (Dietrich et al., 2013; Lee et al., 2021). The evidence we collected on sex differences in OB and amygdalar APE1 expression adds to this body of knowledge under conditions of Lewy body disease.

Study Limitations:

First, a thorough kinetic study might have revealed some degree of early-stage DNA damage and a progressive evolution of repair mechanisms, as alluded to above. On the other hand, prior reports reveal DNA damage in the nigrostriatal pathway *as late as 4 months* after fibril infusions in the striatum (Milanese et al., 2018). A second limitation of our work is the use of whole-tissue extracts in the Glyco-SPOT and ExSy-SPOT assays, as both mitochondrial and nuclear compartments conduct base excision repair. However, dissections of the mouse OB/AON do not yield much tissue for fractionation experiments, and the use of bulk extracts

of postmortem human samples was unavoidable. A third potential limitation of the human samples included high postmortem intervals, but we add that no correlation of postmortem interval with any measure was found. The fourth limitation is that some of the age-matched control subjects died of causes that damage the brain, but this was unavoidable. In the latter context, a strength of animal work is that confounding effects of brain damage in the control group are avoided. Therefore, similarities in the sex-specific patterns of APE1 expression in mice and humans exposed to α-synucleinopathic conditions mitigate this caveat. A fifth limitation is the use of PBS as a control. As mentioned above, we abandoned use of monomeric α-synuclein, because we and others (Patterson et al., 2019; Paumier et al., 2015) have found that monomers provoke low levels of $pSer129^{+}$ pathology, which fails to model unaffected controls. Even if the monomers are handled in a manner (*e.g.*, centrifugation) that provokes virtually no inclusion formation (Polinski et al., 2018), monomeric α-synuclein may modulate the phagocytotic capacities and phenotypic status of microglia (Haenseler et al., 2017; Li et al., 2020; Park et al., 2008) and may stimulate the calcium pump in the plasma membrane (Kowalski et al., 2022).

The major weakness of our work is we have not tested the *in vivo* impact of sex hormones or the function of Y-chromosome genes, which may exert powerful effects on fibril exposure-induced DNA repair and APE1 expression changes. Other groups have shown that estrogen acts directly as a deaggregase when it encounters exogenous fibrils (Hirohata et al., 2009). Given the direct effects of estrogen on fibrils, it may be difficult to determine if estrogen simply reduces the degree of exposure to the original fibril insult via direct disaggregation, or if estrogen tempers the biological *response* to the exogenous fibrils (or a combination of both). In our hands, APE1 expression data were quite consistent from mice to humans—*despite* the postmenopausal status of the female human subjects (aged 65 to 86) and the young or middle-aged rodents employed here. The consistency of our findings across species and age groups may suggest at least some degree of independence from gonadal hormone status. We had initiated a pilot study with escalating concentrations of ß-estradiol in primary hippocampal cultures treated with vehicle or fibrils, but we did not observe any changes in APE1 expression with ß-estradiol exposure *in vitro.* Rodents do not experience menopause, but they go through estropause (Koebele and Bimonte-Nelson, 2016). Further *in vivo* work on APE1 and base excision repair as a function of age (and estropause) is warranted.

Our animal model involves modest (or no) cell loss, and discrepancies with prior work likely depend on the anatomical subregions infused and assessed, as well as the mouse strain and sonication protocols (Mason et al., 2019; Milanese et al., 2018; Nouraei et al., 2018). As articulated previously (Mason et al., 2019), it is important to examine early-stage disease models, as therapeutic interventions become more difficult to test after neurons are irretrievably lost. Based on regression analyses, neurodegeneration does not need to be as severe as widely held before a clinical syndrome is expressed (Cheng et al., 2010). Severe cell loss may also select for ‘super-survivor’ cells that escape death but are not representative of the initial cellular population. The latter arguments provide additional rationale for modest rather than severe APE1 knockdown, as APE1 is essential for survival (Xanthoudakis et al., 1996).

Data in our animal model often show high variance; this was also evident in our previous *in vivo* work (Bhatia et al., 2021; Mason et al., 2016; Mason et al., 2019; Nouraei et al., 2018). We believe the variance is partly related to use of outbred CD-1 mice rather than inbred and genetically more homogeneous C57BL/6 strains, as well as the heterogeneity of the infusion site per unit area, compared to the large mouse striatum, the more common site of preformed fibril infusions in the literature. Voelkl, Wuerbel, and colleagues have argued that consistent observations made in heterogeneous models are more likely to translate across species because they are not overly "standardized" (Richter et al., 2010; Voelkl et al., 2018; Wurbel, 2000). For example, outbred mice, such as CD-1, have higher genetic diversity than inbred strains and are less subject to substrain confounds if the colony is regularly refreshed with breeders from outside sources as we do (Aldinger et al., 2009; Hsieh et al., 2017). In the present study, mice were also experimented on and assayed at a variety of survival periods and ages. In our opinion, cohesiveness of data across heterogeneous protocols may have improved the translatability of the present findings. Likewise, the clinical samples were collected at different institutions by different neuropathologists and varied widely in clinical diagnoses, and *despite this great diversity*, statistical differences in APE1 expression between diseased females and diseased males were noted in combined cohorts.

6. Conclusions

Modest but sex-opposing changes in the DNA repair/redox enzyme APE1 are observed in both mice and humans under conditions of α-synucleinopathic disease. Slight knockdown of APE1 expression or pharmacological inhibition of the DNA repair role of APE1 worsens α-synucleinopathy in hippocampal neurons in the absence of cell loss *in vitro*. Additional studies are needed to parse the biochemical mechanisms whereby loss of APE1 expression or activity regulates inclusion formation, and conversely, how α-synucleinopathic disease modifies APE1 expression according to biological sex. The multifaceted and extranuclear roles of APE1, such as within exosomes (see Intro) must also be accounted for. APE1 has been shown to influence the redox state of a number of transcription factors, including AP-1, NFKB, p53, HIF1, Myb, and Pax (likely through its cysteine residue C65), thereby raising their DNA binding capacities (Gaiddon et al., 1999; Huang et al., 1996; Nishi et al., 2002; Tell et al., 2002; Xanthoudakis and Curran, 1992; Xanthoudakis et al., 1992). If, for example, APE1 binds nuclear α-synuclein or indirectly facilitates the direct attraction of α-synuclein to nuclear DNA (Jiang et al., 2018; Vasudevaraju et al., 2012) through formation of a DNA/protein interactome, then reducing APE1 expression levels or decreasing its function might also impede the DNA binding/bending/repair properties of α-synuclein (Dent et al., 2022; Schaser et al., 2019). These events could raise the concentration of α-synuclein protein within the cytosolic compartment, amplifying the substrate available for fibril-mediated seeding, unfettered inclusion formation, and pathological phosphorylation. Our proof-of-concept work with N-acetylcysteine also suggests that APE1 expression in male cells is influenced by oxidative stress levels or thiol repletion *in vivo*. Hence, future studies are warranted to test if cells with collapse of redox equilibrium, reduced gonadal hormone exposure, and low APE1 expression/activity age faster, suffer catastrophic loss of bioenergetic resources, and fail to react appropriately to additional challenges, such as protein denaturation and aggregation.

Supplementary Material

Refer to Web version on PubMed Central for supplementary material.

Acknowledgements:

We are grateful to Abel Nunez for providing us with photographs of the human brain dissections. Postmortem brain tissue NeuroBioBank specimens were obtained from the Human Brain and Spinal Fluid Resource Center, VA West Los Angeles Healthcare Center (supported by HHSN-271-201300029C and US Department of Veteran Affairs) and the University of Miami Brain Endowment Bank. We thank Sarah Libert for help with the Glyco/ExSy-SPOT and Elizabeth Hurst and Adriana Correa for ARP assay support. We thank the University of Pittsburgh Health Science Sequencing Core at the UPMC Children's Hospital of Pittsburgh for conducting RNA extraction, library preparation, and sequencing on human tissue samples. We are grateful for current and prior NIH grants 1R21NS112671 (RKL), 1R03NS088395-01A1 (RKL), 1R15NS093539-01 (RKL), 1R21NS107960-01 (RKL), 1R21AG068608-01 (RKL), and 1R01NS119528-01 (salary support for LHS).

Data Availability Statement:

The data presented in the manuscript are fully available upon request. Please email leakr@duq.edu.

Abbreviations

A-8oxoG	Adenine-8oxoGuanine
AbaS	abasic sites
ac	anterior commissure
aca	anterior commissure, anterior part
aci	anterior commissure, intrabulbar
acp	anterior commissure, posterior limb
AHi	amygdalohippocampal area
AOD	anterior olfactory area, dorsal
AOE	anterior olfactory nucleus, external
AON	anterior olfactory nucleus
AOP	anterior olfactory area, posterior
AOV	anterior olfactory area, ventral
APir	amygdalopiriform transition area
BER	base excision repair
BLA	basolateral amygdaloid nucleus, anterior part
CA1	cornu Ammonis, field 1
CA2	cornu Ammonis, field 2

CA3	cornu Ammonis, field 3
cc	corpus callosum
CEnt	caudomedial entorhinal cortex
cp	cerebral peduncle
CPD-64	pyrimidine dimers and (6-4) photoproducts
CPu	caudate putamen (striatum)
CxA	cortex-amygdala transition zone
DEn	dorsal endopiriform nucleus
DIEnt	dorsal intermediate entorhinal cortex
DS	dorsal subiculum
ec	external capsule
etheno	alkylated bases
EthA-T	EthenoAdenine-Thymine
fmi	forceps minor of corpus callosum
fmj	forceps major of corpus callosum
fi	fimbria of the hippocampus
GP	globus pallidus
GrDG	granule cell layer of dentate gyrus
GrO	granule cell layer of olfactory bulb
Hx-T	Hypoxanthine-Thymine
ic	internal capsule
IEn	intermediate endopiriform nucleus
lab	longitudinal association bundle
LC	locus coeruleus
LV	lateral ventricle
MEnt	medial entorhinal cortex
ml	medial lemniscus
MPG/AAG	methylpurine DNA glycosylase/3-alkyladenine DNA glycosylase
MoDG	molecular layer of the dentate gyrus

MYH	mutY DNA glycosylase
NEIL	nei-like DNA glycosylase 1
NER	nucleotide excision repair
NTH	endonuclease III
OB	olfactory bulb
opt	optic tract
OGG1	8-Oxogunanine glycosylase
Pir	piriform cortex
PMCo	posteromedial cortical amygdaloid area
Pn	pontine nuclei
S	subiculum
scp	superior cerebellar peduncle
sm	stria medullaris
st	stria terminalis
T-G	Thymine-Guanine
Tg-A	Thymine glycol-Adenine
THF	AP site-Adenine (THF-A)
Tu	olfactory tubercle
U-A	Uracil-Adenine
U-G	Uracil-Guanine, VEn, ventral nucleus of the endopiriform claustrum
VIEnt	ventral intermediate entorhinal cortex
VS	ventral striatum
8oxoG-C	8oxoGuanine-Cytosine

References

Abraham DS, Gruber-Baldini AL, Magder LS, McArdle PF, Tom SE, Barr E, Schrader K, Shulman LM, 2019. Sex differences in Parkinson's disease presentation and progression. Parkinsonism Relat Disord 69, 48–54. [PubMed: 31677455]

Alam ZI, Jenner A, Daniel SE, Lees AJ, Cairns N, Marsden CD, Jenner P, Halliwell B, 1997. Oxidative DNA damage in the parkinsonian brain: an apparent selective increase in 8-hydroxyguanine levels in substantia nigra. Journal of neurochemistry 69, 1196–1203. [PubMed: 9282943]

Aldinger KA, Sokoloff G, Rosenberg DM, Palmer AA, Millen KJ, 2009. Genetic variation and population substructure in outbred CD-1 mice: implications for genome-wide association studies. PLoS One 4, e4729. [PubMed: 19266100]

Anderson JP, Walker DE, Goldstein JM, de Laat R, Banducci K, Caccavello RJ, Barbour R, Huang J, Kling K, Lee M, Diep L, Keim PS, Shen X, Chataway T, Schlossmacher MG, Seubert P, Schenk D, Sinha S, Gai WP, Chilcote TJ, 2006. Phosphorylation of Ser-129 is the dominant pathological modification of alpha-synuclein in familial and sporadic Lewy body disease. J Biol Chem 281, 29739–29752. [PubMed: 16847063]

Antoniali G, Serra F, Lirussi L, Tanaka M, D'Ambrosio C, Zhang S, Radovic S, Dalla E, Ciani Y, Scaloni A, Li M, Piazza S, Tell G, 2017. Mammalian APE1 controls miRNA processing and its interactome is linked to cancer RNA metabolism. Nat Commun 8, 797. [PubMed: 28986522]

Attems J, Toledo JB, Walker L, Gelpi E, Gentleman S, Halliday G, Hortobagyi T, Jellinger K, Kovacs GG, Lee EB, Love S, McAleese KE, Nelson PT, Neumann M, Parkkinen L, Polvikoski T, Sikorska B, Smith C, Grinberg LT, Thal DR, Trojanowski JQ, McKeith IG, 2021. Neuropathological consensus criteria for the evaluation of Lewy pathology in post-mortem brains: a multi-centre study. Acta Neuropathol 141, 159–172. [PubMed: 33399945]

Baek H, Lim CS, Byun HS, Cho HS, Lee YR, Shin YS, Kim HW, Jeon BH, Kim DW, Hong J, Hur GM, Park JB, 2016. The anti-inflammatory role of extranuclear apurinic/apyrimidinic endonuclease 1/redox effector factor-1 in reactive astrocytes. Mol Brain 9, 99. [PubMed: 27986089]

Barchiesi A, Bazzani V, Jabczynska A, Borowski LS, Oeljeklaus S, Warscheid B, Chacinska A, Szczesny RJ, Vascotto C, 2021. DNA Repair Protein APE1 Degrades Dysfunctional Abasic mRNA in Mitochondria Affecting Oxidative Phosphorylation. J Mol Biol 433, 167125. [PubMed: 34224750]

Barzilai A, Biton S, Shiloh Y, 2008. The role of the DNA damage response in neuronal development, organization and maintenance. DNA Repair (Amst) 7, 1010–1027. [PubMed: 18458000]

Basu S, Je G, Kim YS, 2015. Transcriptional mutagenesis by 8-oxodG in alpha-synuclein aggregation and the pathogenesis of Parkinson's disease. Exp Mol Med 47, e179. [PubMed: 26315598]

Beach TG, Adler CH, Lue L, Sue LI, Bachalakuri J, Henry-Watson J, Sasse J, Boyer S, Shirohi S, Brooks R, Eschbacher J, White CL 3rd, Akiyama H, Caviness J, Shill HA, Connor DJ, Sabbagh MN, Walker DG, Arizona Parkinson's Disease C, 2009a. Unified staging system for Lewy body disorders: correlation with nigrostriatal degeneration, cognitive impairment and motor dysfunction. Acta Neuropathol 117, 613–634. [PubMed: 19399512]

Beach TG, Adler CH, Sue LI, Peirce JB, Bachalakuri J, Dalsing-Hernandez JE, Lue LF, Caviness JN, Connor DJ, Sabbagh MN, Walker DG, 2008. Reduced striatal tyrosine hydroxylase in incidental Lewy body disease. Acta Neuropathol 115, 445–451. [PubMed: 17985144]

Beach TG, White CL 3rd, Hladik CL, Sabbagh MN, Connor DJ, Shill HA, Sue LI, Sasse J, Bachalakuri J, Henry-Watson J, Akiyama H, Adler CH, Arizona Parkinson's Disease C, 2009b. Olfactory bulb alpha-synucleinopathy has high specificity and sensitivity for Lewy body disorders. Acta Neuropathol 117, 169–174. [PubMed: 18982334]

Berman AE, Chan WY, Brennan AM, Reyes RC, Adler BL, Suh SW, Kauppinen TM, Edling Y, Swanson RA, 2011. N-acetylcysteine prevents loss of dopaminergic neurons in the EAAC1−/− mouse. Ann Neurol 69, 509–520. [PubMed: 21446024]

Bernstein AI, Garrison SP, Zambetti GP, O'Malley KL, 2011. 6-OHDA generated ROS induces DNA damage and p53- and PUMA-dependent cell death. Mol Neurodegener 6, 2. [PubMed: 21211034]

Bhatia TN, Clark RN, Needham PG, Miner KM, Jamenis AS, Eckhoff EA, Abraham N, Hu X, Wipf P, Luk KC, Brodsky JL, Leak RK, 2021. Heat Shock Protein 70 as a Sex-Skewed Regulator of alpha-Synucleinopathy. Neurotherapeutics 18, 2541–2564. [PubMed: 34528172]

Bobola MS, Finn LS, Ellenbogen RG, Geyer JR, Berger MS, Braga JM, Meade EH, Gross ME, Silber JR, 2005. Apurinic/apyrimidinic endonuclease activity is associated with response to radiation and chemotherapy in medulloblastoma and primitive neuroectodermal tumors. Clin Cancer Res 11, 7405–7414. [PubMed: 16243814]

Braak H, Del Tredici K, Rub U, de Vos RA, Jansen Steur EN, Braak E, 2003. Staging of brain pathology related to sporadic Parkinson's disease. Neurobiol Aging 24, 197–211. [PubMed: 12498954]

Broen MPG, Leentjens AFG, Hinkle JT, Moonen AJH, Kuijf ML, Fischer NM, Perepezko K, Bakker A, Pontone GM, 2018. Clinical Markers of Anxiety Subtypes in Parkinson Disease. J Geriatr Psychiatry Neurol 31, 55–62. [PubMed: 29528763]

Caston RA, Gampala S, Armstrong L, Messmann RA, Fishel ML, Kelley MR, 2021. The multifunctional APE1 DNA repair-redox signaling protein as a drug target in human disease. Drug Discov Today 26, 218–228. [PubMed: 33148489]

Chen DS, Herman T, Demple B, 1991. Two distinct human DNA diesterases that hydrolyze 3'-blocking deoxyribose fragments from oxidized DNA. Nucleic Acids Res 19, 5907–5914. [PubMed: 1719484]

Chen J, Jin K, Chen M, Pei W, Kawaguchi K, Greenberg DA, Simon RP, 1997. Early detection of DNA strand breaks in the brain after transient focal ischemia: implications for the role of DNA damage in apoptosis and neuronal cell death. Journal of neurochemistry 69, 232–245. [PubMed: 9202315]

Cheng HC, Ulane CM, Burke RE, 2010. Clinical progression in Parkinson disease and the neurobiology of axons. Ann Neurol 67, 715–725. [PubMed: 20517933]

Choi S, Lee YR, Park MS, Joo HK, Cho EJ, Kim HS, Kim CS, Park JB, Irani K, Jeon BH, 2013. Histone deacetylases inhibitor trichostatin A modulates the extracellular release of APE1/Ref-1. Biochem Biophys Res Commun 435, 403–407. [PubMed: 23665318]

Clark J, Clore EL, Zheng K, Adame A, Masliah E, Simon DK, 2010. Oral N-acetyl-cysteine attenuates loss of dopaminergic terminals in alpha-synuclein overexpressing mice. PLoS One 5, e12333. [PubMed: 20808797]

Cohen G, Heikkila RE, 1974. The generation of hydrogen peroxide, superoxide radical, and hydroxyl radical by 6-hydroxydopamine, dialuric acid, and related cytotoxic agents. J Biol Chem 249, 2447–2452. [PubMed: 4362682]

Commins DL, Shaughnessy RA, Axt KJ, Vosmer G, Seiden LS, 1989. Variability among brain regions in the specificity of 6-hydroxydopamine (6-OHDA)-induced lesions. J Neural Transm 77, 197–210. [PubMed: 2503586]

Crum TS, Gleixner AM, Posimo JM, Mason DM, Broeren MT, Heinemann SD, Wipf P, Brodsky JL, Leak RK, 2015. Heat shock protein responses to aging and proteotoxicity in the olfactory bulb. J Neurochem 133, 780–794. [PubMed: 25640060]

De Miranda BR, Fazzari M, Rocha EM, Castro S, Greenamyre JT, 2019. Sex Differences in Rotenone Sensitivity Reflect the Male-to-Female Ratio in Human Parkinson's Disease Incidence. Toxicol Sci 170, 133–143. [PubMed: 30907971]

De Miranda BR, Greenamyre JT, 2019. Response to Rotenone and Parkinson's Disease; Reduced Sensitivity in Females. Toxicol Sci 170, 563. [PubMed: 31161199]

Dent SE, King DP, Osterberg VR, Adams EK, Mackiewicz MR, Weissman TA, Unni VK, 2022. Phosphorylation of the aggregate-forming protein alpha-synuclein on serine-129 inhibits its DNA-bending properties. J Biol Chem 298, 101552. [PubMed: 34973339]

Di Maso V, Avellini C, Croce LS, Rosso N, Quadrifoglio F, Cesaratto L, Codarin E, Bedogni G, Beltrami CA, Tell G, Tiribelli C, 2007. Subcellular localization of APE1/Ref-1 in human hepatocellular carcinoma: possible prognostic significance. Mol Med 13, 89–96. [PubMed: 17515960]

Dickson DW, Fujishiro H, DelleDonne A, Menke J, Ahmed Z, Klos KJ, Josephs KA, Frigerio R, Burnett M, Parisi JE, Ahlskog JE, 2008. Evidence that incidental Lewy body disease is pre-symptomatic Parkinson's disease. Acta Neuropathol 115, 437–444. [PubMed: 18264713]

Dietrich AK, Humphreys GI, Nardulli AM, 2013. 17beta-estradiol increases expression of the oxidative stress response and DNA repair protein apurinic endonuclease (Ape1) in the cerebral cortex of female mice following hypoxia. J Steroid Biochem Mol Biol 138, 410–420. [PubMed: 23907014]

Domenis R, Bergamin N, Gianfranceschi G, Vascotto C, Romanello M, Rigo S, Vagnarelli G, Faggiani M, Parodi P, Kelley MR, Beltrami CA, Cesselli D, Tell G, Beltrami AP, 2014. The redox function of APE1 is involved in the differentiation process of stem cells toward a neuronal cell fate. PLoS One 9, e89232. [PubMed: 24586617]

Dragunow M, 1995. Ref-1 expression in adult mammalian neurons and astrocytes. Neurosci Lett 191, 189–192. [PubMed: 7644143]

Fan Z, Beresford PJ, Zhang D, Xu Z, Novina CD, Yoshida A, Pommier Y, Lieberman J, 2003. Cleaving the oxidative repair protein Ape1 enhances cell death mediated by granzyme A. Nat Immunol 4, 145–153. [PubMed: 12524539]

Farr SA, Poon HF, Dogrukol-Ak D, Drake J, Banks WA, Eyerman E, Butterfield DA, Morley JE, 2003. The antioxidants alpha-lipoic acid and N-acetylcysteine reverse memory impairment and brain oxidative stress in aged SAMP8 mice. Journal of neurochemistry 84, 1173–1183. [PubMed: 12603840]

Flores-Cuadrado A, Saiz-Sanchez D, Mohedano-Moriano A, Lamas-Cenjor E, Leon-Olmo V, Martinez-Marcos A, Ubeda-Banon I, 2021. Astrogliosis and sexually dimorphic neurodegeneration and microgliosis in the olfactory bulb in Parkinson's disease. NPJ Parkinsons Dis 7, 11. [PubMed: 33479244]

Forestier A, Sarrazy F, Caillat S, Vandenbrouck Y, Sauvaigo S, 2012. Functional DNA repair signature of cancer cell lines exposed to a set of cytotoxic anticancer drugs using a multiplexed enzymatic repair assay on biochip. PLoS One 7, e51754. [PubMed: 23300565]

Fortini P, Dogliotti E, 2010. Mechanisms of dealing with DNA damage in terminally differentiated cells. Mutat Res 685, 38–44. [PubMed: 19941876]

Frye CA, Petralia SM, Rhodes ME, 2000. Estrous cycle and sex differences in performance on anxiety tasks coincide with increases in hippocampal progesterone and 3alpha,5alpha-THP. Pharmacol Biochem Behav 67, 587–596. [PubMed: 11164090]

Fujiwara H, Hasegawa M, Dohmae N, Kawashima A, Masliah E, Goldberg MS, Shen J, Takio K, Iwatsubo T, 2002. alpha-Synuclein is phosphorylated in synucleinopathy lesions. Nat Cell Biol 4, 160–164. [PubMed: 11813001]

Gaiddon C, Moorthy NC, Prives C, 1999. Ref-1 regulates the transactivation and pro-apoptotic functions of p53 in vivo. EMBO J 18, 5609–5621. [PubMed: 10523305]

Garcia-Esparcia P, Hernandez-Ortega K, Koneti A, Gil L, Delgado-Morales R, Castano E, Carmona M, Ferrer I, 2015. Altered machinery of protein synthesis is region- and stage-dependent and is associated with alpha-synuclein oligomers in Parkinson's disease. Acta Neuropathol Commun 3, 76. [PubMed: 26621506]

Gardner EL, 2011. Addiction and brain reward and antireward pathways. Advances in psychosomatic medicine 30, 22–60. [PubMed: 21508625]

Gater R, Tansella M, Korten A, Tiemens BG, Mavreas VG, Olatawura MO, 1998. Sex differences in the prevalence and detection of depressive and anxiety disorders in general health care settings: report from the World Health Organization Collaborative Study on Psychological Problems in General Health Care. Arch Gen Psychiatry 55, 405–413. [PubMed: 9596043]

Gencer M, Dasdemir S, Cakmakoglu B, Cetinkaya Y, Varlibas F, Tireli H, Kucukali CI, Ozkok E, Aydin M, 2012. DNA repair genes in Parkinson's disease. Genet Test Mol Biomarkers 16, 504–507. [PubMed: 22224629]

Ghosh S, Won SJ, Wang J, Fong R, Butler NJM, Moss A, Wong C, Pan J, Sanchez J, Huynh A, Wu L, Manfredsson FP, Swanson RA, 2021. alpha-synuclein aggregates induce c-Abl activation and dopaminergic neuronal loss by a feed-forward redox stress mechanism. Prog Neurobiol 202, 102070. [PubMed: 33951536]

Goedert M, Spillantini MG, Del Tredici K, Braak H, 2013. 100 years of Lewy pathology. Nat Rev Neurol 9, 13–24. [PubMed: 23183883]

Goldman SM, Tanner CM, 2019. Rotenone and Parkinson's Disease: Reduced Sensitivity in Females. Toxicol Sci 170, 562–563. [PubMed: 31161209]

Goncalves S, Outeiro TF, 2013. Assessing the subcellular dynamics of alpha-synuclein using photoactivation microscopy. Mol Neurobiol 47, 1081–1092. [PubMed: 23389286]

Gonzalez-Hunt CP, Sanders LH, 2020. DNA damage and repair in Parkinson's disease: Recent advances and new opportunities. J Neurosci Res.

Gordon FJ, Brody MJ, Johnson AK, 1985. Regional depletion of central nervous system catecholamines: effects on blood pressure and drinking behavior. Brain Res 345, 285–297. [PubMed: 3930004]

Gross M, Pinhasov A, 2016. Chronic mild stress in submissive mice: Marked polydipsia and social avoidance without hedonic deficit in the sucrose preference test. Behav Brain Res 298, 25–34. [PubMed: 26522843]

Gu X, Cun Y, Li M, Qing Y, Jin F, Zhong Z, Dai N, Qian C, Sui J, Wang D, 2013. Human apurinic/apyrimidinic endonuclease siRNA inhibits the angiogenesis induced by X-ray irradiation in lung cancer cells. Int J Med Sci 10, 870–882. [PubMed: 23781133]

Haaxma CA, Bloem BR, Borm GF, Oyen WJ, Leenders KL, Eshuis S, Booij J, Dluzen DE, Horstink MW, 2007. Gender differences in Parkinson's disease. J Neurol Neurosurg Psychiatry 78, 819–824. [PubMed: 17098842]

Haenseler W, Zambon F, Lee H, Vowles J, Rinaldi F, Duggal G, Houlden H, Gwinn K, Wray S, Luk KC, Wade-Martins R, James WS, Cowley SA, 2017. Excess alpha-synuclein compromises phagocytosis in iPSC-derived macrophages. Sci Rep 7, 9003. [PubMed: 28827786]

Harding AJ, Stimson E, Henderson JM, Halliday GM, 2002. Clinical correlates of selective pathology in the amygdala of patients with Parkinson's disease. Brain 125, 2431–2445. [PubMed: 12390970]

Harsing LG Jr., Zigmond MJ, 1996. Dopaminergic inhibition of striatal GABA release after 6-hydroxydopamine. Brain Res 738, 142–145. [PubMed: 8949937]

Heinemann SD, Posimo JM, Mason DM, Hutchison DF, Leak RK, 2016. Synergistic stress exacerbation in hippocampal neurons: Evidence favoring the dual-hit hypothesis of neurodegeneration. Hippocampus 26, 980–994. [PubMed: 26934478]

Hew-Butler T, Smith-Hale V, Pollard-McGrandy A, VanSumeren M, 2019. Of Mice and Men-The Physiology, Psychology, and Pathology of Overhydration. Nutrients 11.

Hirohata M, Ono K, Morinaga A, Ikeda T, Yamada M, 2009. Anti-aggregation and fibril-destabilizing effects of sex hormones on alpha-synuclein fibrils in vitro. Exp Neurol 217, 434–439. [PubMed: 19289119]

Holmay MJ, Terpstra M, Coles LD, Mishra U, Ahlskog M, Oz G, Cloyd JC, Tuite PJ, 2013. N-Acetylcysteine boosts brain and blood glutathione in Gaucher and Parkinson diseases. Clin Neuropharmacol 36, 103–106. [PubMed: 23860343]

Hsieh LS, Wen JH, Miyares L, Lombroso PJ, Bordey A, 2017. Outbred CD1 mice are as suitable as inbred C57BL/6J mice in performing social tasks. Neurosci Lett 637, 142–147. [PubMed: 27871995]

Huang E, Qu D, Zhang Y, Venderova K, Haque ME, Rousseaux MW, Slack RS, Woulfe JM, Park DS, 2010. The role of Cdk5-mediated apurinic/apyrimidinic endonuclease 1 phosphorylation in neuronal death. Nat Cell Biol 12, 563–571. [PubMed: 20473298]

Huang LE, Arany Z, Livingston DM, Bunn HF, 1996. Activation of hypoxia-inducible transcription factor depends primarily upon redox-sensitive stabilization of its alpha subunit. J Biol Chem 271, 32253–32259. [PubMed: 8943284]

Humphries MD, Prescott TJ, 2010. The ventral basal ganglia, a selection mechanism at the crossroads of space, strategy, and reward. Progress in neurobiology 90, 385–417. [PubMed: 19941931]

Iacono D, Geraci-Erck M, Rabin ML, Adler CH, Serrano G, Beach TG, Kurlan R, 2015. Parkinson disease and incidental Lewy body disease: Just a question of time? Neurology 85, 1670–1679. [PubMed: 26468408]

Iannuzzelli K, Bakker C, Alshaikh J, Bang J, Butala A, Marvel C, Moukheiber E, Murthy M, Pantelyat A, Pletnikova O, Pontone G, Suarez-Cedeno G, Troncoso J, Mills K, Dawson T, Rosenthal L, 2020. Gender Differences in Distribution of Lewy Body Pathology in Individuals with Parkinson's Disease (4664). Neurology 94, 4664.

Jedinak A, Dudhgaonkar S, Kelley MR, Sliva D, 2011. Apurinic/Apyrimidinic endonuclease 1 regulates inflammatory response in macrophages. Anticancer Res 31, 379–385. [PubMed: 21378315]

Jiang K, Rocha S, Westling A, Kesarimangalam S, Dorfman KD, Wittung-Stafshede P, Westerlund F, 2018. Alpha-Synuclein Modulates the Physical Properties of DNA. Chemistry 24, 15685–15690. [PubMed: 30102440]

Kam TI, Mao X, Park H, Chou SC, Karuppagounder SS, Umanah GE, Yun SP, Brahmachari S, Panicker N, Chen R, Andrabi SA, Qi C, Poirier GG, Pletnikova O, Troncoso JC, Bekris LM,

Leverenz JB, Pantelyat A, Ko HS, Rosenthal LS, Dawson TM, Dawson VL, 2018. Poly(ADP-ribose) drives pathologic alpha-synuclein neurodegeneration in Parkinson's disease. Science 362.

Katz M, Won SJ, Park Y, Orr A, Jones DP, Swanson RA, Glass GA, 2015. Cerebrospinal fluid concentrations of N-acetylcysteine after oral administration in Parkinson's disease. Parkinsonism Relat Disord 21, 500–503. [PubMed: 25765302]

Keefe KA, Stricker EM, Zigmond MJ, Abercrombie ED, 1990. Environmental stress increases extracellular dopamine in striatum of 6-hydroxydopamine-treated rats: in vivo microdialysis studies. Brain Res 527, 350–353. [PubMed: 2123730]

Khedr EM, Abdelrahman AA, Elserogy Y, Zaki AF, Gamea A, 2020. Depression and anxiety among patients with Parkinson's disease: frequency, risk factors, and impact on quality of life. The Egyptian Journal of Neurology, Psychiatry and Neurosurgery 56, 116.

Kikuchi A, Takeda A, Onodera H, Kimpara T, Hisanaga K, Sato N, Nunomura A, Castellani RJ, Perry G, Smith MA, Itoyama Y, 2002. Systemic increase of oxidative nucleic acid damage in Parkinson's disease and multiple system atrophy. Neurobiol Dis 9, 244–248. [PubMed: 11895375]

Kim WC, King D, Lee CH, 2010. RNA-cleaving properties of human apurinic/apyrimidinic endonuclease 1 (APE1). Int J Biochem Mol Biol 1, 12–25. [PubMed: 21968700]

Koebele SV, Bimonte-Nelson HA, 2016. Modeling menopause: The utility of rodents in translational behavioral endocrinology research. Maturitas 87, 5–17. [PubMed: 27013283]

Kowalski A, Betzer C, Larsen ST, Gregersen E, Bermejo MC, Jensen PH, Nissen P, 2022. Monomeric α-Synuclein activates the Plasma Membrane Calcium Pump. bioRxiv, 2022.2002.2021.481193.

Krohn K, Maier J, Paschke R, 2007. Mechanisms of disease: hydrogen peroxide, DNA damage and mutagenesis in the development of thyroid tumors. Nat Clin Pract Endocrinol Metab 3, 713–720. [PubMed: 17893690]

Krokan HE, Bjoras M, 2013. Base excision repair. Cold Spring Harb Perspect Biol 5, a012583. [PubMed: 23545420]

Kume K, Kikukawa M, Hanyu H, Takata Y, Umahara T, Sakurai H, Kanetaka H, Ohyashiki K, Ohyashiki JH, Iwamoto T, 2012. Telomere length shortening in patients with dementia with Lewy bodies. Eur J Neurol 19, 905–910. [PubMed: 22288427]

Lai CY, Hsieh LL, Tang R, Santella RM, Chang-Chieh CR, Yeh CC, 2016. Association between polymorphisms of APE1 and OGG1 and risk of colorectal cancer in Taiwan. World J Gastroenterol 22, 3372–3380. [PubMed: 27022219]

Leak RK, Li P, Zhang F, Sulaiman HH, Weng Z, Wang G, Stetler RA, Shi Y, Cao G, Gao Y, Chen J, 2015. Apurinic/apyrimidinic endonuclease 1 upregulation reduces oxidative DNA damage and protects hippocampal neurons from ischemic injury. Antioxid Redox Signal 22, 135–148. [PubMed: 24180454]

Lee J, Pinares-Garcia P, Loke H, Ham S, Vilain E, Harley VR, 2019. Sex-specific neuroprotection by inhibition of the Y-chromosome gene, SRY, in experimental Parkinson's disease. Proc Natl Acad Sci U S A 116, 16577–16582. [PubMed: 31371505]

Lee SK, Chung JI, Park MS, Joo HK, Lee EJ, Cho EJ, Park JB, Ryoo S, Irani K, Jeon BH, 2011. Apurinic/apyrimidinic endonuclease 1 inhibits protein kinase C-mediated p66shc phosphorylation and vasoconstriction. Cardiovasc Res 91, 502–509. [PubMed: 21467074]

Lee YR, Joo HK, Lee EO, Kim S, Jin H, Choi YH, Kim CS, Jeon BH, 2021. 17beta-Estradiol Increases APE1/Ref-1 Secretion in Vascular Endothelial Cells and Ovariectomized Mice: Involvement of Calcium-Dependent Exosome Pathway. Biomedicines 9.

Lehmkuhl AM, Dirr ER, Fleming SM, 2014. Olfactory assays for mouse models of neurodegenerative disease. J Vis Exp, e51804. [PubMed: 25177842]

Li J, Gu CZ, Su JB, Zhu LH, Zhou Y, Huang HY, Liu CF, 2016. Changes in Olfactory Bulb Volume in Parkinson's Disease: A Systematic Review and Meta-Analysis. PLoS One 11, e0149286. [PubMed: 26900958]

Li M, Wilson DM 3rd, 2014. Human apurinic/apyrimidinic endonuclease 1. Antioxid Redox Signal 20, 678–707. [PubMed: 23834463]

Li N, Stewart T, Sheng L, Shi M, Cilento EM, Wu Y, Hong JS, Zhang J, 2020. Immunoregulation of microglial polarization: an unrecognized physiological function of alpha-synuclein. J Neuroinflammation 17, 272. [PubMed: 32943057]

Li P, Hu X, Gan Y, Gao Y, Liang W, Chen J, 2011. Mechanistic insight into DNA damage and repair in ischemic stroke: exploiting the base excision repair pathway as a model of neuroprotection. Antioxidants & redox signaling 14, 1905–1918. [PubMed: 20677909]

Liu R, Umbach DM, Peddada SD, Xu Z, Troster AI, Huang X, Chen H, 2015. Potential sex differences in nonmotor symptoms in early drug-naive Parkinson disease. Neurology 84, 2107–2115. [PubMed: 25925983]

Lo YL, Jou YS, Hsiao CF, Chang GC, Tsai YH, Su WC, Chen KY, Chen YM, Huang MS, Hu CY, Chen CJ, Hsiung CA, 2009. A polymorphism in the APE1 gene promoter is associated with lung cancer risk. Cancer Epidemiol Biomarkers Prev 18, 223–229. [PubMed: 19124501]

Lopez DJ, Rodriguez JA, Banuelos S, 2021. Molecular Mechanisms Regulating the DNA Repair Protein APE1: A Focus on Its Flexible N-Terminal Tail Domain. Int J Mol Sci 22.

Lu GS, Li M, Xu CX, Wang D, 2018. APE1 stimulates EGFR-TKI resistance by activating Akt signaling through a redox-dependent mechanism in lung adenocarcinoma. Cell Death Dis 9, 1111. [PubMed: 30382076]

Lyras L, Perry RH, Perry EK, Ince PG, Jenner A, Jenner P, Halliwell B, 1998. Oxidative damage to proteins, lipids, and DNA in cortical brain regions from patients with dementia with Lewy bodies. J Neurochem 71, 302–312. [PubMed: 9648879]

Ma KL, Song LK, Yuan YH, Zhang Y, Han N, Gao K, Chen NH, 2014. The nuclear accumulation of alpha-synuclein is mediated by importin alpha and promotes neurotoxicity by accelerating the cell cycle. Neuropharmacology 82, 132–142. [PubMed: 23973294]

Malfatti MC, Antoniali G, Codrich M, Tell G, 2021. Coping with RNA damage with a focus on APE1, a BER enzyme at the crossroad between DNA damage repair and RNA processing/decay. DNA Repair (Amst) 104, 103133. [PubMed: 34049077]

Mangiapane G, Parolini I, Conte K, Malfatti MC, Corsi J, Sanchez M, Pietrantoni A, D'Agostino VG, Tell G, 2021. Enzymatically active apurinic/apyrimidinic endodeoxyribonuclease 1 is released by mammalian cells through exosomes. J Biol Chem 296, 100569. [PubMed: 33753167]

Maroteaux L, Campanelli JT, Scheller RH, 1988. Synuclein: a neuron-specific protein localized to the nucleus and presynaptic nerve terminal. J Neurosci 8, 2804–2815. [PubMed: 3411354]

Mason DM, Nouraei N, Pant DB, Miner KM, Hutchison DF, Luk KC, Stolz JF, Leak RK, 2016. Transmission of alpha-synucleinopathy from olfactory structures deep into the temporal lobe. Mol Neurodegener 11, 49. [PubMed: 27363576]

Mason DM, Wang Y, Bhatia TN, Miner KM, Trbojevic SA, Stolz JF, Luk KC, Leak RK, 2019. The center of olfactory bulb-seeded alpha-synucleinopathy is the limbic system and the ensuing pathology is higher in male than in female mice. Brain Pathol 29, 741–770. [PubMed: 30854742]

Mijit M, Caston R, Gampala S, Fishel ML, Fehrenbacher J, Kelley MR, 2021. APE1/Ref-1 - One Target with Multiple Indications: Emerging Aspects and New Directions. J Cell Signal 2, 151–161. [PubMed: 34557865]

Milanese C, Cerri S, Ulusoy A, Gornati SV, Plat A, Gabriels S, Blandini F, Di Monte DA, Hoeijmakers JH, Mastroberardino PG, 2018. Activation of the DNA damage response in vivo in synucleinopathy models of Parkinson's disease. Cell Death Dis 9, 818. [PubMed: 30050065]

Millau JF, Raffin AL, Caillat S, Claudet C, Arras G, Ugolin N, Douki T, Ravanat JL, Breton J, Oddos T, Dumontet C, Sarasin A, Chevillard S, Favier A, Sauvaigo S, 2008. A microarray to measure repair of damaged plasmids by cell lysates. Lab Chip 8, 1713–1722. [PubMed: 18813395]

Montaldo NP, Bordin DL, Brambilla A, Rosinger M, Fordyce Martin SL, Bjoras KO, Bradamante S, Aas PA, Furrer A, Olsen LC, Kunath N, Otterlei M, Saetrom P, Bjoras M, Samson LD, van Loon B, 2019. Alkyladenine DNA glycosylase associates with transcription elongation to coordinate DNA repair with gene expression. Nat Commun 10, 5460. [PubMed: 31784530]

Murray EA, 2007. The amygdala, reward and emotion. Trends Cogn Sci 11, 489–497. [PubMed: 17988930]

Nelson PT, Schmitt FA, Jicha GA, Kryscio RJ, Abner EL, Smith CD, Van Eldik LJ, Markesbery WR, 2010. Association between male gender and cortical Lewy body pathology in large autopsy series. J Neurol 257, 1875–1881. [PubMed: 20563821]

Nishi T, Shimizu N, Hiramoto M, Sato I, Yamaguchi Y, Hasegawa M, Aizawa S, Tanaka H, Kataoka K, Watanabe H, Handa H, 2002. Spatial redox regulation of a critical cysteine residue of NF-kappa B in vivo. J Biol Chem 277, 44548–44556. [PubMed: 12213807]

Nouraei N, Mason DM, Miner KM, Carcella MA, Bhatia TN, Dumm BK, Soni D, Johnson DA, Luk KC, Leak RK, 2018. Critical appraisal of pathology transmission in the alpha-synuclein fibril model of Lewy body disorders. Exp Neurol 299, 172–196. [PubMed: 29056362]

Nouraei N, Zarger L, Weilnau JN, Han J, Mason DM, Leak RK, 2016. Investigation of the therapeutic potential of N-acetyl cysteine and the tools used to define nigrostriatal degeneration in vivo. Toxicol Appl Pharmacol 296, 19–30. [PubMed: 26879220]

Oliveira LMA, Gasser T, Edwards R, Zweckstetter M, Melki R, Stefanis L, Lashuel HA, Sulzer D, Vekrellis K, Halliday GM, Tomlinson JJ, Schlossmacher M, Jensen PH, Schulze-Hentrich J, Riess O, Hirst WD, El-Agnaf O, Mollenhauer B, Lansbury P, Outeiro TF, 2021. Alpha-synuclein research: defining strategic moves in the battle against Parkinson's disease. NPJ Parkinsons Dis 7, 65. [PubMed: 34312398]

Oliveira TT, Coutinho LG, de Oliveira LOA, Timoteo ARS, Farias GC, Agnez-Lima LF, 2022. APE1/Ref-1 Role in Inflammation and Immune Response. Front Immunol 13, 793096. [PubMed: 35296074]

Paiva I, Pinho R, Pavlou MA, Hennion M, Wales P, Schutz AL, Rajput A, Szego EM, Kerimoglu C, Gerhardt E, Rego AC, Fischer A, Bonn S, Outeiro TF, 2017. Sodium butyrate rescues dopaminergic cells from alpha-synuclein-induced transcriptional deregulation and DNA damage. Human molecular genetics 26, 2231–2246. [PubMed: 28369321]

Park JY, Paik SR, Jou I, Park SM, 2008. Microglial phagocytosis is enhanced by monomeric alpha-synuclein, not aggregated alpha-synuclein: implications for Parkinson's disease. Glia 56, 1215–1223. [PubMed: 18449945]

Park MS, Kim CS, Joo HK, Lee YR, Kang G, Kim SJ, Choi S, Lee SD, Park JB, Jeon BH, 2013. Cytoplasmic localization and redox cysteine residue of APE1/Ref-1 are associated with its anti-inflammatory activity in cultured endothelial cells. Mol Cells 36, 439–445. [PubMed: 24213673]

Patterson JR, Duffy MF, Kemp CJ, Howe JW, Collier TJ, Stoll AC, Miller KM, Patel P, Levine N, Moore DJ, Luk KC, Fleming SM, Kanaan NM, Paumier KL, El-Agnaf OMA, Sortwell CE, 2019. Time course and magnitude of alpha-synuclein inclusion formation and nigrostriatal degeneration in the rat model of synucleinopathy triggered by intrastriatal alpha-synuclein preformed fibrils. Neurobiol Dis 130, 104525. [PubMed: 31276792]

Paumier KL, Luk KC, Manfredsson FP, Kanaan NM, Lipton JW, Collier TJ, Steece-Collier K, Kemp CJ, Celano S, Schulz E, Sandoval IM, Fleming S, Dirr E, Polinski NK, Trojanowski JQ, Lee VM, Sortwell CE, 2015. Intrastriatal injection of pre-formed mouse alpha-synuclein fibrils into rats triggers alpha-synuclein pathology and bilateral nigrostriatal degeneration. Neurobiol Dis 82, 185–199. [PubMed: 26093169]

Pavlou MAS, Pinho R, Paiva I, Outeiro TF, 2017. The yin and yang of alpha-synuclein-associated epigenetics in Parkinson's disease. Brain 140, 878–886. [PubMed: 27585855]

Paxinos G, 2015. The rat nervous system. Elsevier Academic Press: Amsterdam ; Boston.

Paxinos G, Franklin KBJ, 2013. Paxinos and Franklin's The mouse brain in stereotaxic coordinates. Academic Press, an imprint of Elsevier: Amsterdam.

Pearce RK, Hawkes CH, Daniel SE, 1995. The anterior olfactory nucleus in Parkinson's disease. Movement disorders : official journal of the Movement Disorder Society 10, 283–287. [PubMed: 7651444]

Picillo M, Fasano A, 2015. How much does sex matter in Parkinson disease? Neurology 84, 2102–2104. [PubMed: 25925984]

Pinho R, Paiva I, Jercic KG, Fonseca-Ornelas L, Gerhardt E, Fahlbusch C, Garcia-Esparcia P, Kerimoglu C, Pavlou MAS, Villar-Pique A, Szego E, Lopes da Fonseca T, Odoardi F, Soeroes S, Rego AC, Fischle W, Schwamborn JC, Meyer T, Kugler S, Ferrer I, Attems J, Fischer A, Becker S, Zweckstetter M, Borovecki F, Outeiro TF, 2019. Nuclear localization and phosphorylation modulate pathological effects of alpha-synuclein. Human molecular genetics 28, 31–50. [PubMed: 30219847]

Polinski NK, Volpicelli-Daley LA, Sortwell CE, Luk KC, Cremades N, Gottler LM, Froula J, Duffy MF, Lee VMY, Martinez TN, Dave KD, 2018. Best Practices for Generating and Using Alpha-Synuclein Pre-Formed Fibrils to Model Parkinson's Disease in Rodents. J Parkinsons Dis.

Pons B, Belmont AS, Masson-Genteuil G, Chapuis V, Oddos T, Sauvaigo S, 2010. Age-associated modifications of Base Excision Repair activities in human skin fibroblast extracts. Mech Ageing Dev 131, 661–665. [PubMed: 20854835]

Posimo JM, Unnithan AS, Gleixner AM, Choi HJ, Jiang Y, Pulugulla SH, Leak RK, 2014. Viability assays for cells in culture. Journal of visualized experiments : JoVE 83, e50645.

Posimo JM, Weilnau JN, Gleixner AM, Broeren MT, Weiland NL, Brodsky JL, Wipf P, Leak RK, 2015. Heat shock protein defenses in the neocortex and allocortex of the telencephalon. Neurobiol Aging 36, 1924–1937. [PubMed: 25771395]

Prunier C, Masson-Genteuil G, Ugolin N, Sarrazy F, Sauvaigo S, 2012. Aging and photo-aging DNA repair phenotype of skin cells-evidence toward an effect of chronic sun-exposure. Mutat Res 736, 48–55. [PubMed: 21669211]

Przedborski S, Ischiropoulos H, 2005. Reactive oxygen and nitrogen species: weapons of neuronal destruction in models of Parkinson's disease. Antioxid Redox Signal 7, 685–693. [PubMed: 15890013]

Rai G, Vyjayanti VN, Dorjsuren D, Simeonov A, Jadhav A, Wilson DM 3rd, Maloney DJ, 2012. Synthesis, biological evaluation, and structure-activity relationships of a novel class of apurinic/apyrimidinic endonuclease 1 inhibitors. J Med Chem 55, 3101–3112. [PubMed: 22455312]

Rey NL, George S, Steiner JA, Madaj Z, Luk KC, Trojanowski JQ, Lee VM, Brundin P, 2018. Spread of aggregates after olfactory bulb injection of alpha-synuclein fibrils is associated with early neuronal loss and is reduced long term. Acta Neuropathol 135, 65–83. [PubMed: 29209768]

Rey NL, Steiner JA, Maroof N, Luk KC, Madaj Z, Trojanowski JQ, Lee VM, Brundin P, 2016a. Widespread transneuronal propagation of alpha-synucleinopathy triggered in olfactory bulb mimics prodromal Parkinson's disease. J Exp Med.

Rey NL, Wesson DW, Brundin P, 2016b. The olfactory bulb as the entry site for prion-like propagation in neurodegenerative diseases. Neurobiol Dis.

Reyes RC, Cittolin-Santos GF, Kim JE, Won SJ, Brennan-Minnella AM, Katz M, Glass GA, Swanson RA, 2016. Neuronal Glutathione Content and Antioxidant Capacity can be Normalized In Situ by N-acetyl Cysteine Concentrations Attained in Human Cerebrospinal Fluid. Neurotherapeutics 13, 217–225. [PubMed: 26572666]

Richter SH, Garner JP, Auer C, Kunert J, Wurbel H, 2010. Systematic variation improves reproducibility of animal experiments. Nat Methods 7, 167–168. [PubMed: 20195246]

Rocha EM, De Miranda B, Sanders LH, 2018. Alpha-synuclein: Pathology, mitochondrial dysfunction and neuroinflammation in Parkinson's disease. Neurobiol Dis 109, 249–257. [PubMed: 28400134]

Sadakierska-Chudy A, Haduch A, Golembiowska K, Daniel WA, 2010. Effects of low doses of intracerebroventricular 6-OHDA on the levels of monoaminergic neurotransmitters in rat brain structures. Pharmacol Rep 62, 1225–1230. [PubMed: 21273682]

Sancar A, 1994. Mechanisms of DNA excision repair. Science 266, 1954–1956. [PubMed: 7801120]

Sanders LH, McCoy J, Hu X, Mastroberardino PG, Dickinson BC, Chang CJ, Chu CT, Van Houten B, Greenamyre JT, 2014. Mitochondrial DNA damage: molecular marker of vulnerable nigral neurons in Parkinson's disease. Neurobiol Dis 70, 214–223. [PubMed: 24981012]

Sanders LH, Paul KC, Howlett EH, Lawal H, Boppana S, Bronstein JM, Ritz B, Greenamyre JT, 2017. Editor's Highlight: Base Excision Repair Variants and Pesticide Exposure Increase Parkinson's Disease Risk. Toxicol Sci 158, 188–198. [PubMed: 28460087]

Sauvaigo S, Guerniou V, Rapin D, Gasparutto D, Caillat S, Favier A, 2004. An oligonucleotide microarray for the monitoring of repair enzyme activity toward different DNA base damage. Anal Biochem 333, 182–192. [PubMed: 15351295]

Schaser AJ, Osterberg VR, Dent SE, Stackhouse TL, Wakeham CM, Boutros SW, Weston LJ, Owen N, Weissman TA, Luna E, Raber J, Luk KC, McCullough AK, Woltjer RL, Unni VK, 2019. Alpha-synuclein is a DNA binding protein that modulates DNA repair with implications for Lewy body disorders. Sci Rep 9, 10919. [PubMed: 31358782]

Schell H, Hasegawa T, Neumann M, Kahle PJ, 2009. Nuclear and neuritic distribution of serine-129 phosphorylated alpha-synuclein in transgenic mice. Neuroscience 160, 796–804. [PubMed: 19272424]

Sepe S, Milanese C, Gabriels S, Derks KW, Payan-Gomez C, van IWF, Rijksen YM, Nigg AL, Moreno S, Cerri S, Blandini F, Hoeijmakers JH, Mastroberardino PG, 2016. Inefficient DNA Repair Is an Aging-Related Modifier of Parkinson's Disease. Cell Rep 15, 1866–1875. [PubMed: 27210754]

Sevilya Z, Leitner-Dagan Y, Pinchev M, Kremer R, Elinger D, Lejbkowicz F, Rennert HS, Freedman LS, Rennert G, Paz-Elizur T, Livneh Z, 2015. Development of APE1 enzymatic DNA repair assays: low APE1 activity is associated with increase lung cancer risk. Carcinogenesis 36, 982–991. [PubMed: 26045303]

Siddiqui A, Chinta SJ, Mallajosyula JK, Rajagopolan S, Hanson I, Rane A, Melov S, Andersen JK, 2012. Selective binding of nuclear alpha-synuclein to the PGC1alpha promoter under conditions of oxidative stress may contribute to losses in mitochondrial function: implications for Parkinson's disease. Free Radic Biol Med 53, 993–1003. [PubMed: 22705949]

Sorokowski P, Karwowski M, Misiak M, Marczak MK, Dziekan M, Hummel T, Sorokowska A, 2019. Sex Differences in Human Olfaction: A Meta-Analysis. Front Psychol 10, 242. [PubMed: 30814965]

Sorrentino ZA, Goodwin MS, Riffe CJ, Dhillon JS, Xia Y, Gorion KM, Vijayaraghavan N, McFarland KN, Golbe LI, Yachnis AT, Giasson BI, 2019. Unique alpha-synuclein pathology within the amygdala in Lewy body dementia: implications for disease initiation and progression. Acta Neuropathol Commun 7, 142. [PubMed: 31477175]

Soudry Y, Lemogne C, Malinvaud D, Consoli SM, Bonfils P, 2011. Olfactory system and emotion: common substrates. Eur Ann Otorhinolaryngol Head Neck Dis 128, 18–23. [PubMed: 21227767]

Stetler RA, Gao Y, Leak RK, Weng Z, Shi Y, Zhang L, Pu H, Zhang F, Hu X, Hassan S, Ferguson C, Homanics GE, Cao G, Bennett MV, Chen J, 2016. APE1/Ref-1 facilitates recovery of gray and white matter and neurological function after mild stroke injury. Proc Natl Acad Sci U S A 113, E3558–3567. [PubMed: 27274063]

Stoyka LE, Arrant AE, Thrasher DR, Russell DL, Freire J, Mahoney CL, Narayanan A, Dib AG, Standaert DG, Volpicelli-Daley LA, 2020. Behavioral defects associated with amygdala and cortical dysfunction in mice with seeded alpha-synuclein inclusions. Neurobiol Dis 134, 104708. [PubMed: 31837424]

Surguchev AA, Surguchov A, 2017. Synucleins and Gene Expression: Ramblers in a Crowd or Cops Regulating Traffic? Front Mol Neurosci 10, 224. [PubMed: 28751856]

Surguchov A, 2015. Intracellular Dynamics of Synucleins: "Here, There and Everywhere". Int Rev Cell Mol Biol 320, 103–169. [PubMed: 26614873]

Tanner CM, Goldman SM, Ross GW, Grate SJ, 2014. The disease intersection of susceptibility and exposure: chemical exposures and neurodegenerative disease risk. Alzheimers Dement 10, S213–225. [PubMed: 24924672]

Tapias V, Hu X, Luk KC, Sanders LH, Lee VM, Greenamyre JT, 2017. Synthetic alpha-synuclein fibrils cause mitochondrial impairment and selective dopamine neurodegeneration in part via iNOS-mediated nitric oxide production. Cell Mol Life Sci 74, 2851–2874. [PubMed: 28534083]

Tell G, Damante G, Caldwell D, Kelley MR, 2005. The intracellular localization of APE1/Ref-1: more than a passive phenomenon? Antioxidants & redox signaling 7, 367–384. [PubMed: 15706084]

Tell G, Pines A, Paron I, D'Elia A, Bisca A, Kelley MR, Manzini G, Damante G, 2002. Redox effector factor-1 regulates the activity of thyroid transcription factor 1 by controlling the redox state of the N transcriptional activation domain. J Biol Chem 277, 14564–14574. [PubMed: 11834746]

Tell G, Quadrifoglio F, Tiribelli C, Kelley MR, 2009. The many functions of APE1/Ref-1: not only a DNA repair enzyme. Antioxid Redox Signal 11, 601–620. [PubMed: 18976116]

Thakur S, Dhiman M, Tell G, Mantha AK, 2015. A review on protein-protein interaction network of APE1/Ref-1 and its associated biological functions. Cell Biochem Funct 33, 101–112. [PubMed: 25790058]

Tremblay C, Abbasi N, Zeighami Y, Yau Y, Dadar M, Rahayel S, Dagher A, 2020. Sex effects on brain structure in de novo Parkinson's disease: a multimodal neuroimaging study. Brain.

Ubeda-Banon I, Saiz-Sanchez D, de la Rosa-Prieto C, Argandona-Palacios L, Garcia-Munozguren S, Martinez-Marcos A, 2010. alpha-Synucleinopathy in the human olfactory system in Parkinson's disease: involvement of calcium-binding protein- and substance P-positive cells. Acta Neuropathol 119, 723–735. [PubMed: 20383714]

Ubeda-Banon I, Saiz-Sanchez D, de la Rosa-Prieto C, Martinez-Marcos A, 2013. alpha-Synuclein in the olfactory system in Parkinson's disease: role of neural connections on spreading pathology. Brain structure & function.

Valverde M, Lozano-Salgado J, Fortini P, Rodriguez-Sastre MA, Rojas E, Dogliotti E, 2018. Hydrogen Peroxide-Induced DNA Damage and Repair through the Differentiation of Human Adipose-Derived Mesenchymal Stem Cells. Stem Cells Int 2018, 1615497. [PubMed: 30405718]

van de Beek M, Babapour Mofrad R, van Steenoven I, Vanderstichele H, Scheltens P, Teunissen CE, Lemstra AW, van der Flier WM, 2020. Sex-specific associations with cerebrospinal fluid biomarkers in dementia with Lewy bodies. Alzheimers Res Ther 12, 44. [PubMed: 32303272]

Vascotto C, Fantini D, Romanello M, Cesaratto L, Deganuto M, Leonardi A, Radicella JP, Kelley MR, D'Ambrosio C, Scaloni A, Quadrifoglio F, Tell G, 2009. APE1/Ref-1 interacts with NPM1 within nucleoli and plays a role in the rRNA quality control process. Mol Cell Biol 29, 1834–1854. [PubMed: 19188445]

Vasko MR, Guo C, Kelley MR, 2005. The multifunctional DNA repair/redox enzyme Ape1/Ref-1 promotes survival of neurons after oxidative stress. DNA repair 4, 367–379. [PubMed: 15661660]

Vasquez V, Mitra J, Hegde PM, Pandey A, Sengupta S, Mitra S, Rao KS, Hegde ML, 2017. Chromatin-Bound Oxidized alpha-Synuclein Causes Strand Breaks in Neuronal Genomes in in vitro Models of Parkinson's Disease. J Alzheimers Dis 60, S133–S150. [PubMed: 28731447]

Vasudevaraju P, Guerrero E, Hegde ML, Collen TB, Britton GB, Rao KS, 2012. New evidence on alpha-synuclein and Tau binding to conformation and sequence specific GC* rich DNA: Relevance to neurological disorders. J Pharm Bioallied Sci 4, 112–117. [PubMed: 22557921]

Villar-Pique A, Lopes da Fonseca T, Sant'Anna R, Szego EM, Fonseca-Ornelas L, Pinho R, Carija A, Gerhardt E, Masaracchia C, Abad Gonzalez E, Rossetti G, Carloni P, Fernandez CO, Foguel D, Milosevic I, Zweckstetter M, Ventura S, Outeiro TF, 2016. Environmental and genetic factors support the dissociation between alpha-synuclein aggregation and toxicity. Proc Natl Acad Sci U S A 113, E6506–E6515. [PubMed: 27708160]

Voelkl B, Vogt L, Sena ES, Wurbel H, 2018. Reproducibility of preclinical animal research improves with heterogeneity of study samples. PLoS Biol 16, e2003693. [PubMed: 29470495]

Volpicelli-Daley LA, Luk KC, Lee VM, 2014. Addition of exogenous alpha-synuclein preformed fibrils to primary neuronal cultures to seed recruitment of endogenous alpha-synuclein to Lewy body and Lewy neurite-like aggregates. Nat Protoc 9, 2135–2146. [PubMed: 25122523]

Whitaker AM, Freudenthal BD, 2018. APE1: A skilled nucleic acid surgeon. DNA Repair (Amst) 71, 93–100. [PubMed: 30170830]

Wurbel H, 2000. Behaviour and the standardization fallacy. Nat Genet 26, 263. [PubMed: 11062457]

Xanthoudakis S, Curran T, 1992. Identification and characterization of Ref-1, a nuclear protein that facilitates AP-1 DNA-binding activity. The EMBO journal 11, 653–665. [PubMed: 1537340]

Xanthoudakis S, Miao G, Wang F, Pan YC, Curran T, 1992. Redox activation of Fos-Jun DNA binding activity is mediated by a DNA repair enzyme. EMBO J 11, 3323–3335. [PubMed: 1380454]

Xanthoudakis S, Smeyne RJ, Wallace JD, Curran T, 1996. The redox/DNA repair protein, Ref-1, is essential for early embryonic development in mice. Proc Natl Acad Sci U S A 93, 8919–8923. [PubMed: 8799128]

Yoon YS, You JS, Kim TK, Ahn WJ, Kim MJ, Son KH, Ricarte D, Ortiz D, Lee SJ, Lee HJ, 2022. Senescence and impaired DNA damage responses in alpha-synucleinopathy models. Exp Mol Med 54, 115–128. [PubMed: 35136202]

Zaky A, Bouali-Benazzouz R, Favereaux A, Tell G, Landry M, 2018. APE1/Ref-1 redox function contributes to inflammatory pain sensitization. Exp Neurol 307, 1–11. [PubMed: 29772245]

Zhang J, Perry G, Smith MA, Robertson D, Olson SJ, Graham DG, Montine TJ, 1999. Parkinson's disease is associated with oxidative damage to cytoplasmic DNA and RNA in substantia nigra neurons. Am J Pathol 154, 1423–1429. [PubMed: 10329595]

Zhou M, Xu S, Mi J, Ueda K, Chan P, 2013. Nuclear translocation of alpha-synuclein increases susceptibility of MES23.5 cells to oxidative stress. Brain Res 1500, 19–27. [PubMed: 23337620]

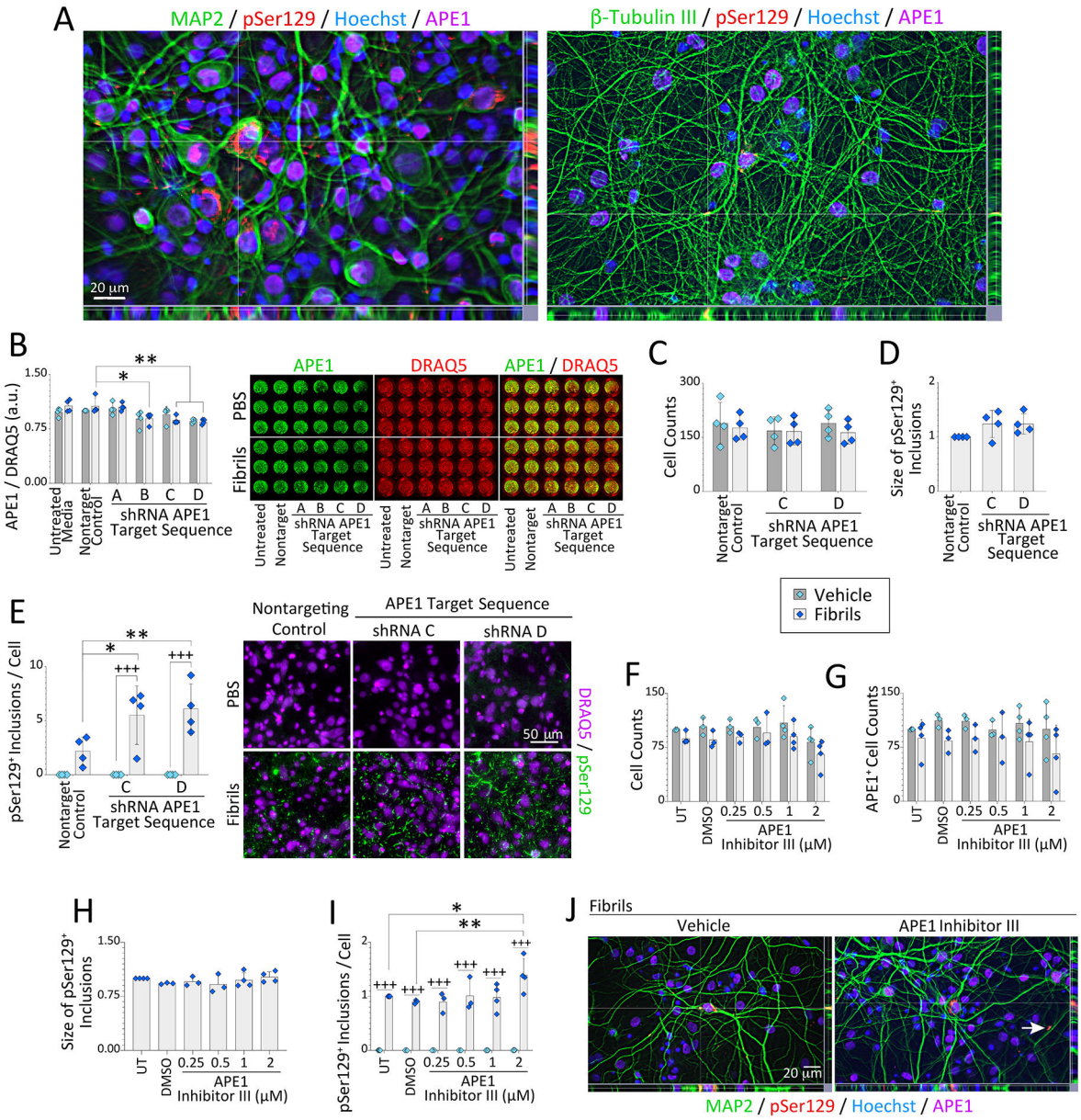

Figure 1. Loss of APE1 exacerbates α-synucleinopathy without cell loss.

(**A**) Primary hippocampal cultures were treated on day *in vitro* 2 (DIV2) with sonicated, preformed α-synuclein fibrils (1 μg/mL) and immunostained on DIV12 for somatodendritic neuron marker MAP2, neuronal process marker β-tubulin III, APE1, and phosphorylated α-synuclein (pSer129; *also see* Fig. S1-S2). Nuclei were stained with the Hoechst reagent. (**B-E**) Primary hippocampal cultures were treated on DIV2 with α-synuclein fibrils (1 μg/mL) and APE1-targeted shRNA by lentiviral delivery (60,000 transduction units per well in 96-well plates). Cells were fixed three days (**B**) or 10 days (**C-E**) after lentiviral exposure and stained for pan-nuclear markers DRAQ5 or Hoechst (*also see* Fig. S3-S5). (**B**) APE1 levels are shown as a fraction of DRAQ5^{+} nuclear staining on DIV5 via In-Cell Western analyses on a 16-bit, low resolution/high sensitivity infrared imager. (**C-E**) Microscopic quantification of DRAQ5^{+} cell counts, pSer129^{+} inclusion sizes (fold-

change of nontargeting controls), and pSer129$^+$ inclusion densities on DIV12 after APE1 knockdown. **(F-J)** Primary hippocampal cultures were treated on DIV2 with α-synuclein fibrils (1 μg/mL) and APE1 Inhibitor III. Cells were immunostained on DIV12 for pSer129 and APE1 (*see* Fig. S6). **(F)** Hoechst$^+$ cell counts and **(G)** APE1$^+$ cell counts as % of untreated controls. **(H)** pSer129$^+$ inclusion size (fold-change of untreated controls). **(I)** pSer129$^+$ inclusion counts as a fraction of Hoechst$^+$ cell numbers (fold-change of untreated controls). (**J**) Subcellular localization of the inclusions was not changed by APE1 inhibitor III treatment (Fig. S1D *for higher-resolution images and reference to white arrow*). Data are shown as mean ± S.D. of 3-4 independent cultures. For **B-I**, two-way ANOVAs were followed by the Bonferroni *post hoc* (except **D** and **H**, which were analyzed with one-way ANOVA/Bonferroni). For **B-E**, *$p \leq 0.05$, **$p \leq 0.01$ shRNA vs. non-targeting lentivirus control; +++$p \leq 0.001$ vehicle vs. fibrils. For **F-I**, *$p \leq 0.05$, **$p \leq 0.01$ APE1 inhibitor III vs. untreated (UT) or DMSO controls; +++$p \leq 0.001$ vehicle vs. fibrils.

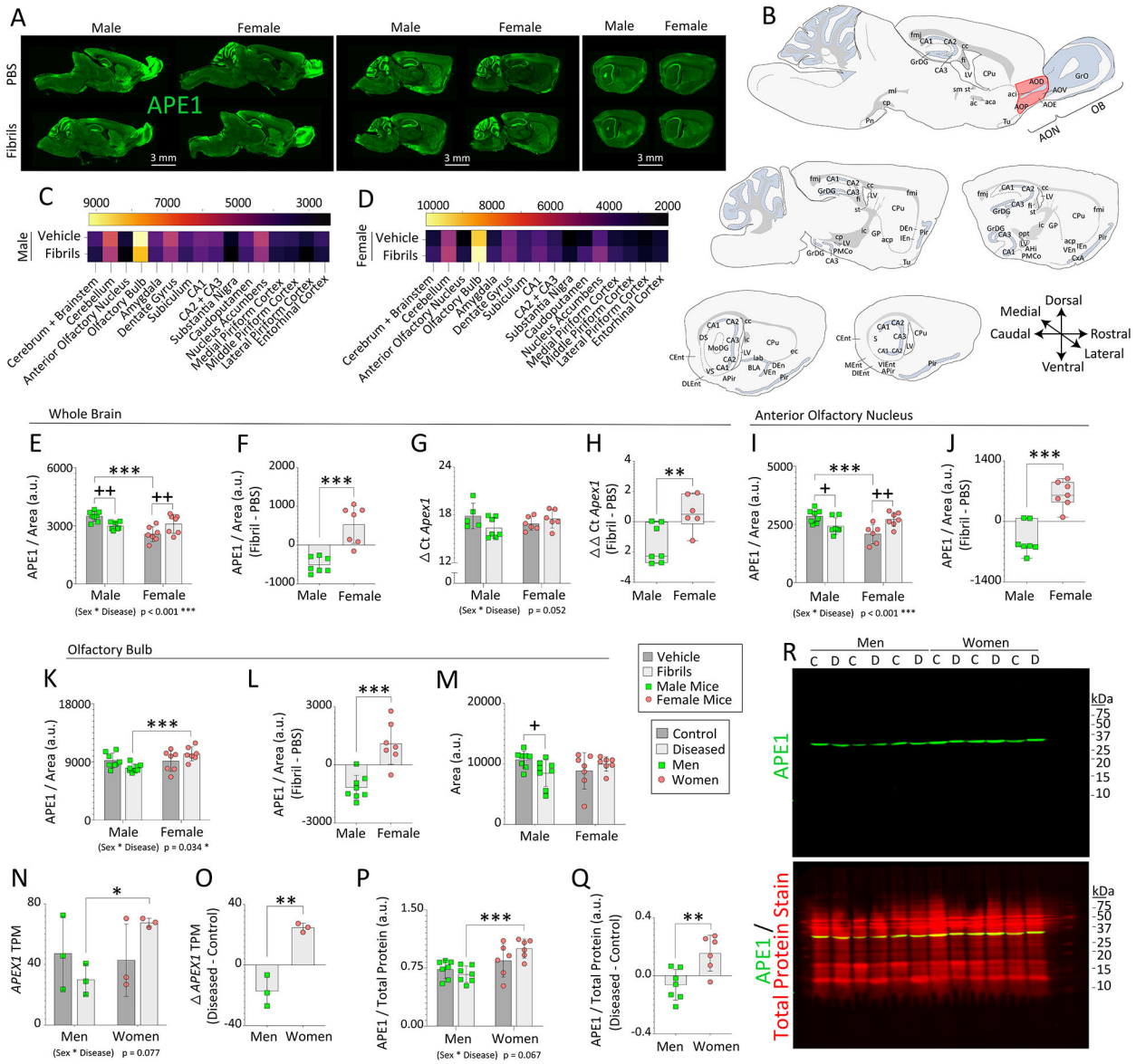

Figure 2. Impact of α-synucleinopathy on APE1 expression in mice and humans.

Three-month-old male and female mice were infused in the right OB/AON with sonicated α-synuclein fibrils (5 μg) or an equal volume of PBS (1 μL). Sagittal brain sections were collected and immunostained for APE1 after a six-month survival period. A blinded observer analyzed APE1 expression and the area of select brain regions by tracing the region of interest in the right hemisphere on **(A)** low-resolution, high-sensitivity scans captured with a 16 bit-depth imager. **(B)** Manual sketches of sagittal brain sections with anatomical regions of interest (red shading = AON). **(C-D)** Heatmaps of average APE1 signal per unit area. APE1 expression levels per unit area in traces of the mouse **(E)** whole brain, **(I)** AON, and **(K)** OB. Differential expression of APE1 elicited by fibril infusions within the mouse **(F)** whole brain, **(J)** AON, and **(L)** OB (*see* Fig. S8). **(M)** Average size of the traced outline of the mouse OB. **(G-H)** Eight-month-old male and female mice were bilaterally infused in the OB/AON with α-synuclein fibrils or PBS. Three months later, APE1 mRNA levels

were assessed by RT-qPCR in whole-brain extracts **(G)**. **(H)** Global APE1 mRNA levels expressed as the difference between fibril and PBS-infused animals. **(N-R)** The UCLA and University of Miami Brain Banks provided human OB samples from deceased male and female control subjects and subjects diagnosed with Lewy body disorders (see demographics in Table S3 in (Bhatia et al., 2021)). Bulk RNA Smart-Sequencing was performed on the UCLA samples, and transcripts per million (TPM) for the *APEX1* gene are shown in **N**. **(O)** Differential expression of *APEX1* TPM in the OB of subjects with Lewy body disorders compared to unaffected controls. **(P)** APE1 expression in the human OB from UCLA and Miami cohorts was determined by Western immunoblotting and expressed as a fraction of total protein levels (REVERT stain from LI-COR). **(Q)** Differential APE1 protein expression levels in the human OB of subjects with Lewy body disorders compared to unaffected controls. **(R)** Full-length immunoblots depicting APE1 and total protein expression. The entire lane of the Total Protein REVERT stain was quantified (*for assay validation see* Fig. S9 *and for brighter images of blots see* Fig. S10). Data in panels **E-Q** are shown as the mean ± S.D. (except box plots with interquartile ranges in **H** and **J**). Two-way ANOVAs in **E, G, I, K, M, N,** and **P** were followed by the Bonferroni *post hoc*, and statistical interactions between biological sex and disease are noted below respective graphs. For **F**, **L**, **O**, and **Q**, two-tailed Student's *t* tests were performed. The Mann-Whitney U test was performed in **H** and **J**. *$p \leq 0.05$, **$p \leq 0.01$, ***$p \leq 0.001$ male vs. female; +$p \leq 0.05$, ++$p \leq 0.01$ PBS vs. fibrils.

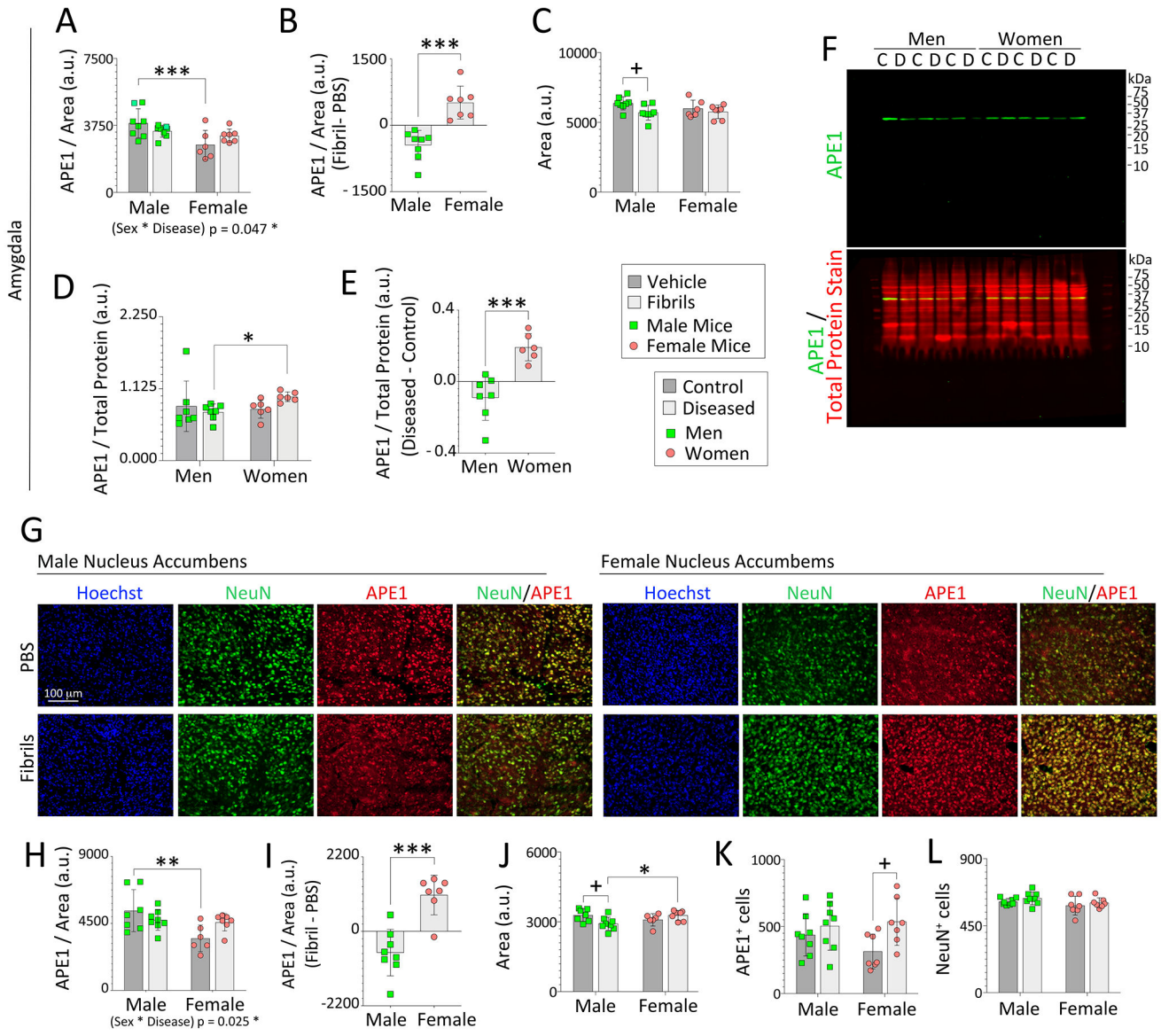

Figure 3. Impact of α-synucleinopathy on APE1 expression in the amygdala of mice and humans and in the mouse nucleus accumbens.

Three-month-old male and female mice were infused in the right OB/AON with sonicated α-synuclein fibrils (5 µg) or an equal volume of PBS (1 µL). Brain sections were cut in the sagittal plane after a six-month survival period and immunostained for APE1 or NeuN. Nuclei were labeled with Hoechst. A blinded observer analyzed APE1 expression levels and area of select regions by tracing the area of interest in the right hemisphere on scans captured with a 16 bit-depth, low-resolution imager (*images in* Fig. 2A). APE1 levels per unit area in traces of the mouse **(A)** amygdala and **(H)** nucleus accumbens. **(B, I)** Differential expression of APE1 protein within the mouse amygdala and accumbens after fibril infusions. Average size of the traced outline of the mouse **(C)** amygdala and **(J)** accumbens in sagittal sections. **(D-F)** APE1 expression in the human amygdala from the UCLA and University of Miami cohorts was determined by Western immunoblotting

and expressed as a fraction of total protein levels in **D** (*see* Fig. S9, S10, *and* S11). **(E)** Differential expression of APE1 protein in the amygdala of subjects with Lewy body disorders compared to unaffected controls. **(F)** Full-length immunoblots depicting APE1 and total protein expression. The entire lane of the Total Protein REVERT stain was quantified. **(G)** Representative images of the mouse nucleus accumbens. A blinded observer performed counts of **(K)** $APE1^+$ and **(L)** $NeuN^+$ cells per field of view in the nucleus accumbens. Note that the APE1 immunostaining in the female accumbens in the PBS group is notably weaker than in PBS-infused males, as is also evident in the quantified data, and was captured at high exposures with low contrast to visualize virtually all signal plus background. Data in panels **A**, **C**, **D**, **H**, and **J-L** are shown as the mean ± S.D. Two-way ANOVAs were followed by the Bonferroni *post hoc* in panels **A**, **C**, **H**, and **J-L**, and the Kruskal-Wallis was followed by the Dunn's test in panel **D** (*also see parametric tests in* Fig. S11A-B). Statistical interactions between biological sex and the disease model are noted below respective graphs. Data in **B, E**, and **I** were analyzed by the two-tailed Student's *t* test. *$p \leq 0.05$, **$p \leq 0.01$, ***$p \leq 0.001$ male vs. female; +$p \leq 0.05$ PBS vs. fibrils (mice) or control vs. diseased (humans).

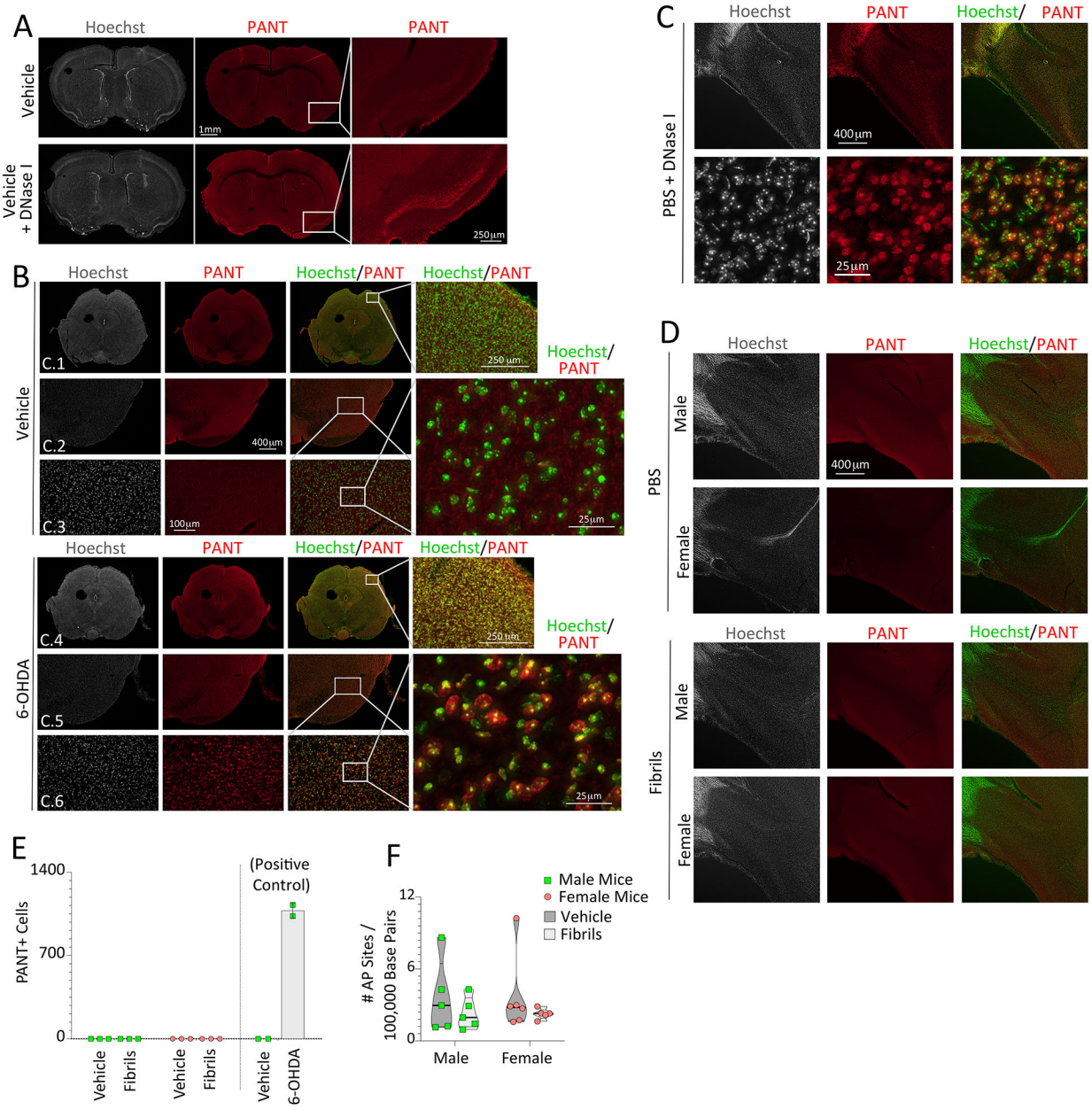

Figure 4. α-synucleinopathy does not elicit robust DNA damage in limbic structures, in contrast to 6-OHDA infusions in the mouse striatum.

(A-B) DNA polymerase I-mediated biotin-dATP nick translation (PANT) labeling of single-stranded DNA breaks was used to assess DNA damage in three-month-old male mice one week following striatal infusions of 6-hydroxydopamine (6-OHDA; 4 µg) or an equal volume of 0.02% ascorbic acid in saline (1.6 µL). DNase I was briefly applied to adjacent brain sections as a positive control (as in **A**). The Hoechst reagent was applied to stain all nuclei. Rows C.1 and C.4: Representative images of the mesencephalon. Rows C.2 + C.5 and C.3 + C.6: Images of the ventral mesencephalon at increasing magnification. **(C-D)** PANT labeling on sagittal brain sections from male and female mice bilaterally infused in the OB/AON at three months of age with fibrils or PBS and assayed six months later. **(C)**

DNase I-treated sagittal sections of the AON from a PBS-infused male mouse, captured with 4× (top row) and 20× (bottom row) objectives. **(D)** Representative images of the AON from PBS and fibril-infused male and female mice. (**E**) $PANT^{+}$ cell counts per field of view in the AON of vehicle (PBS) or fibril-infused mice (n=3 per group) and in the ventral mesencephalon of vehicle (ascorbic acid in PBS) or 6-OHDA-infused mice (n=2 per group). No statistical tests were performed on the right side of panel **E** given the n of 2 mice in the 6-OHDA/vehicle groups. Data are shown as mean ± S.D. (**F**) Eight-month-old male and female mice were bilaterally infused in the OB/AON with sonicated α-synuclein fibrils (5 μg) or an equal volume of PBS (1 μL). Three months later, DNA from the right piriform cortex was harvested for assessment of apurinic/apyrimidinic (AP) sites using a biotin-tagged aldehyde-reactive probe. Violin plots in panel **F** illustrate interquartile ranges as horizontal lines and density estimations of data distributions as the plot width (not statistically significant, either by parametric two-way ANOVA or by nonparametric one-way Kruskal-Wallis test).

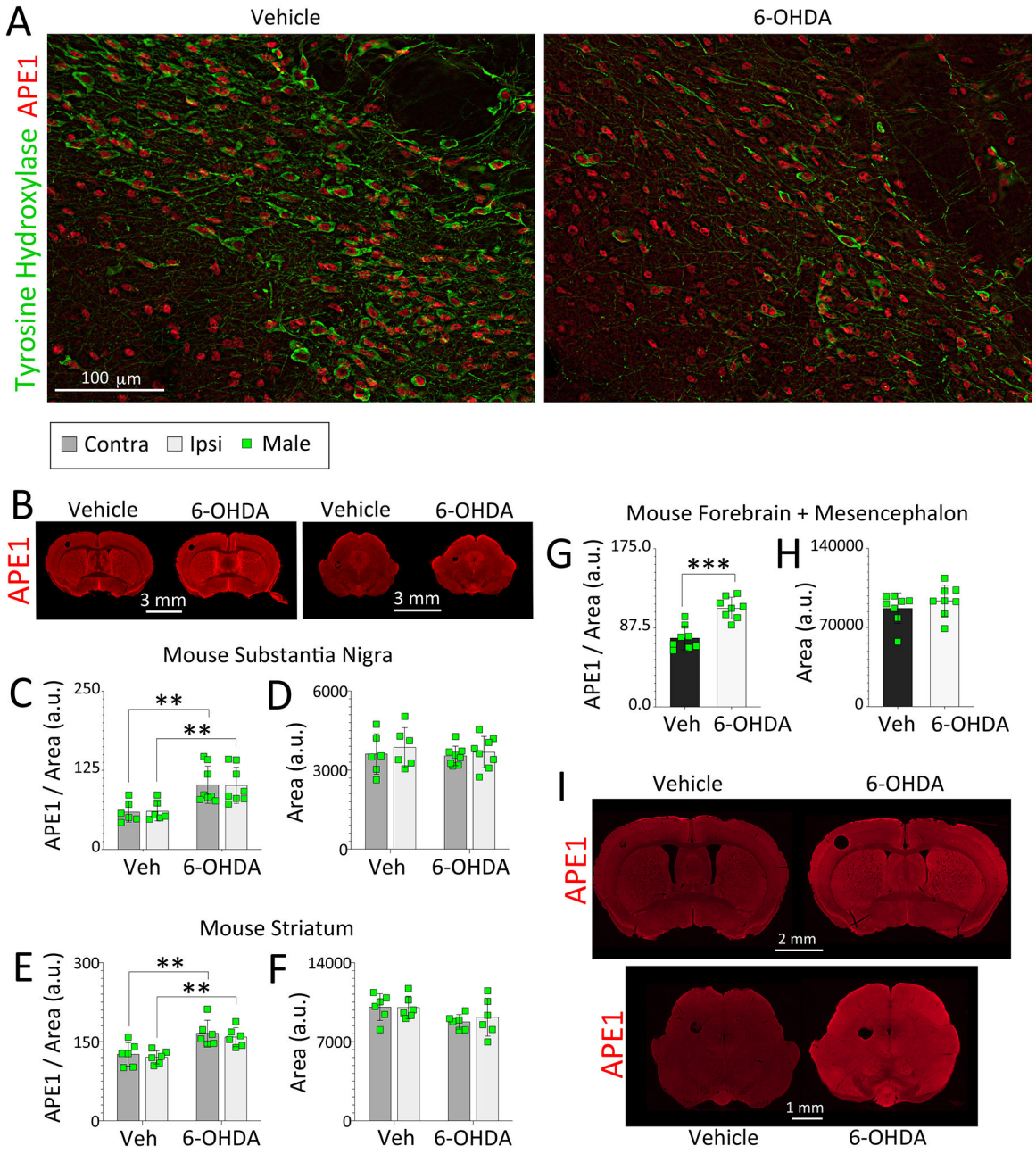

Figure 5. 6-hydroxydopamine-induced oxidative stress increases APE1 expression in male mice.

Three-month-old male mice were infused in the right striatum with 6-OHDA (4 µg) or an equivalent volume of 0.02% ascorbic acid in saline (1.6 µL). One week following infusions, coronal brain sections were collected and immunostained for APE1 and the dopaminergic marker tyrosine hydroxylase (TH). **(A)** APE1 and TH colocalization within dopaminergic neurons in the substantia nigra. A blinded observer analyzed APE1 expression levels and area of the **(C-D)** substantia nigra, **(E-F)** striatum, and **(G-H)** forebrain and mesencephalon by tracing the regions of interest on **(B)** low-resolution, high-sensitivity scans captured with a 16 bit-depth imager. **(I)** Microscopic images were also stitched to form high-resolution photomontages of entire coronal brain sections. Data in **C-H** are shown as the mean ±

S.D. Two-way ANOVAs were followed by the Bonferroni in **C-F**. For **G** and **H**, two-tailed Student's *t* tests were performed. $^{**}p \leq 0.01$, $^{***}p \leq 0.001$ ascorbic acid in saline vehicle (Veh) vs. 6-OHDA.

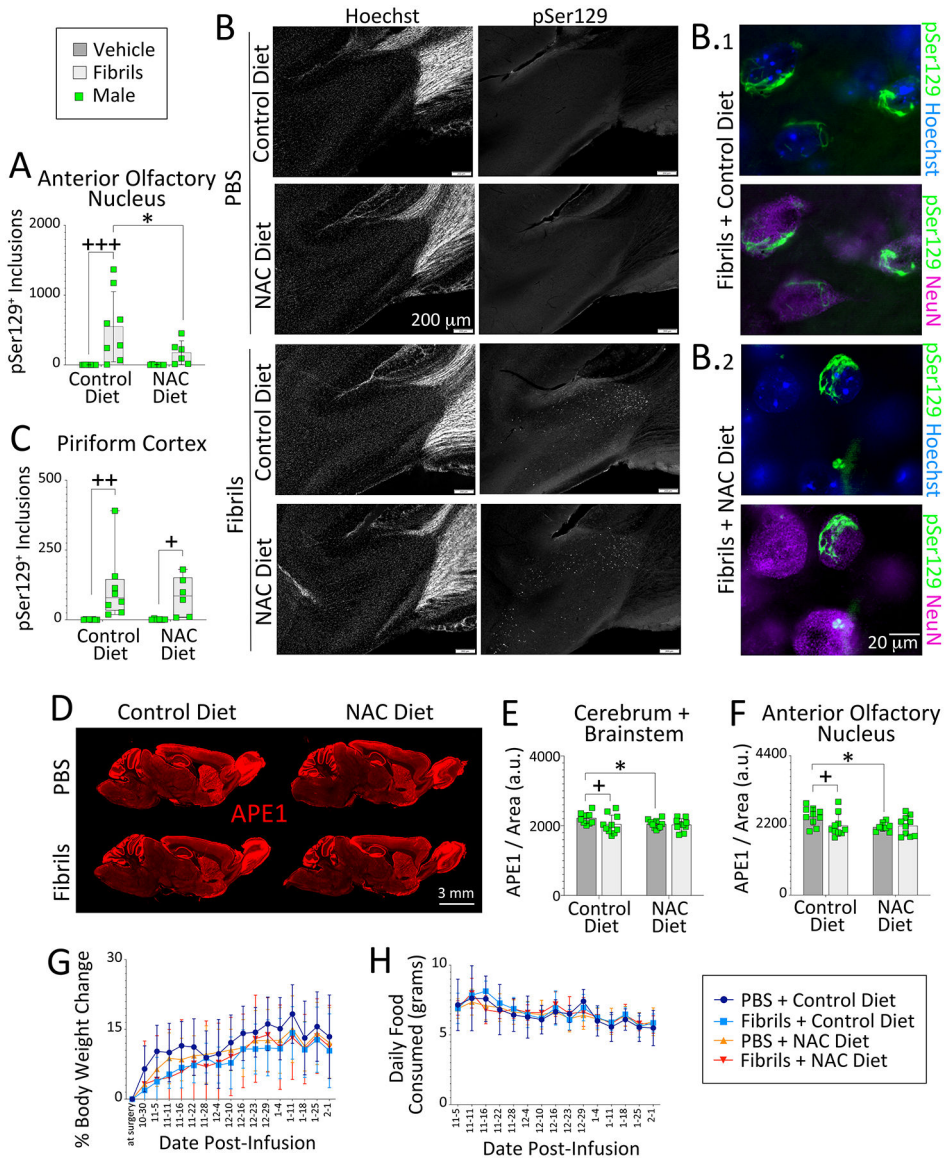

Figure 6. Oxidative stress influences APE1 expression in male mice.

Four-month-old male mice were infused in the right OB/AON with sonicated α-synuclein fibrils (5 μg) or PBS (1 μL). Mouse chow with and without N-acetylcysteine (~200 mg NAC/kg bodyweight) was administered for three months following fibril or PBS infusions. Sagittal brain sections were collected after a three-month survival period at 7 months of age and immunostained for pSer129 and APE1. **(A)** A blinded observer counted pSer129^{+} structures per field of view in the **(A-B)** AON and **(C)** piriform cortex of the right hemisphere. Higher magnification images of inclusions in the AON of fibril-infused animals are shown in B.1-2, vis-à-vis nuclear staining with NeuN antibodies or the Hoechst reagent (*also see* Fig. S14-S15). (**D-F**) A blinded observer analyzed APE1 expression levels in the **(E)** cerebrum and brainstem, as well as in the **(F)** AON of the right hemisphere by tracing the regions of interest on **(D)** low-resolution, high-sensitivity scans captured with a 16 bit-depth imager. Line graphs showing **(G)** % bodyweight change and **(H)** daily food

consumption as a function of days post-infusion. Data in panels **A** and **E-F** are shown as the mean ± S.D. Two-way ANOVAs were followed by the Bonferroni *post hoc*. Data in **C** are shown are box plots with interquartile ranges, analyzed by the Kruskal-Wallis test and Dunn *post hoc*. *$p \leq 0.05$ Control vs. NAC diet; + $p \leq 0.05$, ++ $p \leq 0.01$, +++$p \leq 0.001$ PBS vs. fibrils.

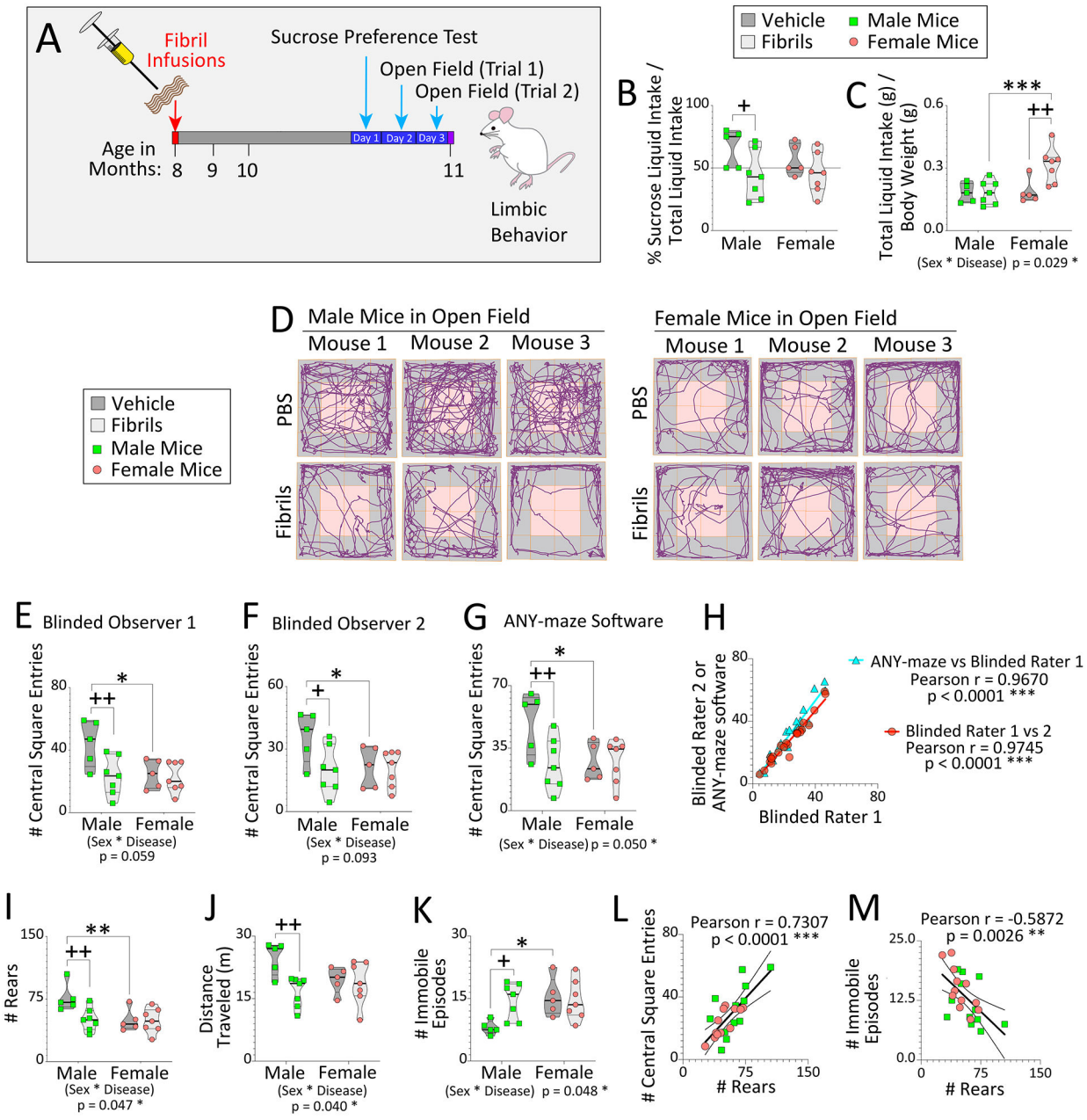

Figure 7. Biological sex modifies the impact of α-synucleinopathy on some types of limbic and motor-related behaviors in mice.

Eight-month-old male and female mice were bilaterally infused in the OB/AON with sonicated α-synuclein fibrils (5 μg) or an equivalent volume of PBS (1 μL). **(A)** Three months later, animals were subject to the sucrose preference and open field tests (time not drawn to scale). **(B)** Preference for sucrose water over regular drinking water and **(C)** total liquid intake were assessed over 24 hours. **(D-M)** Two, 5-minute trials in open fields were carried out on consecutive days. All subsequent graphs illustrate the average of the two open field trials. **(D)** Representative track plots of three mice from each group. **(E-F)** Two independently trained observers and **(G)** the ANY-maze behavior tracking software recorded

the number of times each mouse entered a central square, shaded pink in panel D. **(H)** The blinded raters' results were correlated with each other and with ANY-maze output. A blinded observer recorded **(I)** the number of rears, and ANY-maze software was used to assess **(J)** distance traveled in meters (m), and **(K)** number of immobile episodes. The number of rears was positively correlated with **(L)** the number of central square entries and inversely correlated with **(M)** the number of immobile episodes. Violin plots in panels **B-C**, **E-G**, and **I-K** illustrate interquartile ranges as horizontal lines and density estimations of data distributions as plot widths. Two-way ANOVAs were followed by the Bonferroni *post hoc*; *$p \leq 0.05$, **$p \leq 0.01$, ***$p \leq 0.001$ male vs. female; +$p \leq 0.05$, ++$p \leq 0.01$ PBS vs. fibrils. For **H** and **L-M**, data were analyzed with Pearson's correlation test (two-sided); **$p \leq 0.01$, ***$p \leq 0.001$.

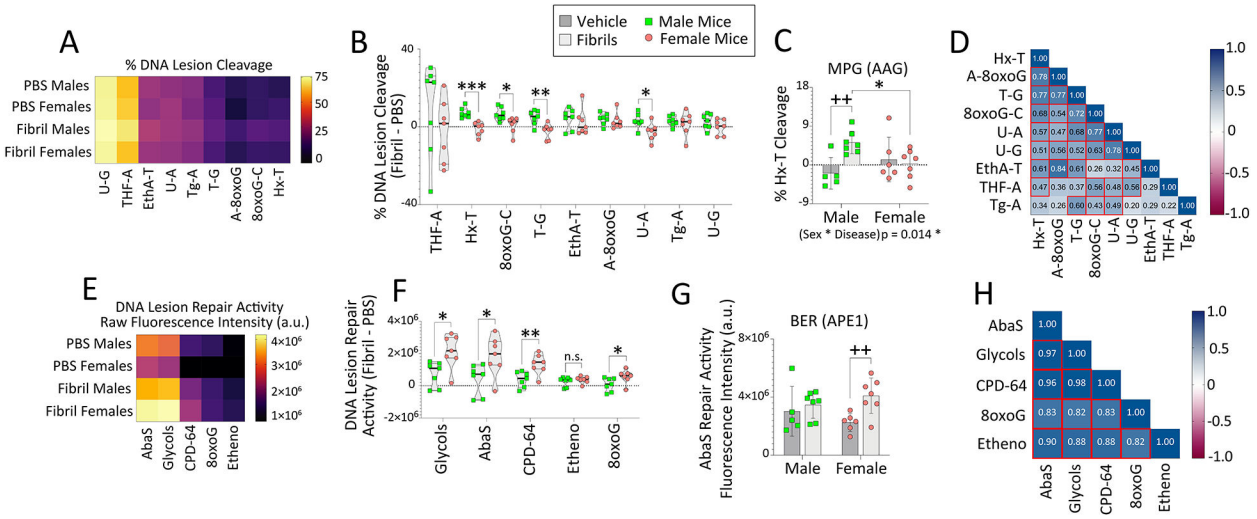

Figure 8. Fibril-infused female mice display inducible DNA repair activities for oxidative DNA lesions.

Eight-month-old male and female mice were bilaterally infused in the OB/AON with sonicated α-synuclein fibrils (5 μg) or an equal volume of PBS (1 μL). The OB/AON was collected for the Glyco-SPOT and ExSy-SPOT assays three months later. **(A-D)** For the Glyco-SPOT, excision/cleavage of synthetic, specific DNA lesions was measured. **(A)** Heatmap depicting the mean excision of each Glyco-SPOT lesion. **(B)** Differential DNA cleavage elicited by fibril infusions in males *vs.* females. Percentage cleavage of **(C)** Hx-T lesions, repaired by the enzyme MPG (also known as AAG). **(D)** Correlation matrix heatmap depicting correlation coefficients between each variable assessed by the Glyco-SPOT for all animals. Heatmap cells with red borders denote correlations ($p \leq 0.05$). **(E-H)** For the ExSy-SPOT, the incorporation of nucleotide substrates into the repair of a lesioned DNA plasmid by base excision and nucleotide excision repair pathways was measured on a functionalized biochip. **(E)** Heatmap depicting mean repair capacity for each ExSy-SPOT lesion. **(F)** Differential DNA repair elicited by fibril infusions in males *vs.* females. **(G)** Raw fluorescence data showing repair of abasic sites by APE1. **(H)** Correlation matrix heatmap depicting correlation coefficients between each variable assessed by the ExSy-SPOT for all animals. Heatmap cells with red borders denote correlations ($p \leq 0.05$). Data in **C** and **G** are shown as the mean ± S.D. Violin plots in **B** and **F** illustrate interquartile ranges as horizontal lines and density estimations of data distributions as plot widths. Two-way ANOVAs in **C** and **G** were followed by the Bonferroni *post hoc*. For **B** and **F**, two-tailed Student's *t* tests were performed. *$p \leq 0.05$, **$p \leq 0.01$, ***$p \leq 0.001$ male vs. female; ++$p \leq 0.01$ PBS vs. fibrils. For **D** and **H**, data were analyzed with Pearson's correlation test (two-sided).